Acta Biomaterialia 183 (2024) 111–129

Contents lists available at ScienceDirect

Acta Biomaterialia

journal homepage: www.elsevier.com/locate/actbio

Full length article

In vitro throughput screening of anticancer drugs using patient-derived cell lines cultured on vascularized three-dimensional stromal tissues

Yuki Takahashi[a,b,1], Rii Morimura[a,b,1], Kei Tsukamoto[a], Sayaka Gomi[a], Asuka Yamada[a,c], Miki Mizukami[a], Yasuyuki Naito[a,c], Shinji Irie[c], Satoshi Nagayama[d,e], Eiji Shinozaki[f], Kensei Yamaguchi[f], Naoya Fujita[g], Shiro Kitano[a,c,*], Ryohei Katayama[h,**], Michiya Matsusaki[c,i,***]

[a] *Business Development Division, Technical Research Institute, TOPPAN Holdings Inc., Saitama 345-8508, Japan*
[b] *Division of Clinical Chemotherapy, Cancer Chemotherapy Center, Japanese Foundation for Cancer Research, Tokyo 135-8550, Japan*
[c] *Joint Research Laboratory (TOPPAN) for Advanced Cell Regulatory Chemistry, Graduate School of Engineering, Osaka University, Osaka 565-0871, Japan*
[d] *Department of Colorectal Surgery, Gastroenterological Cancer Center, The Cancer Institute Hospital, Japanese Foundation for Cancer Research, Tokyo 135-8550, Japan*
[e] *Department of Surgery, Uji Tokushukai Medical Center, Kyoto 611-0041, Japan*
[f] *Department of Gastroenterological Chemotherapy, The Cancer Institute Hospital, Japanese Foundation for Cancer Research, Tokyo 135-8550, Japan*
[g] *Cancer Chemotherapy Center, Japanese Foundation for Cancer Research, Tokyo 135-8550, Japan*
[h] *Division of Experimental Chemotherapy, Cancer Chemotherapy Center, Japanese Foundation for Cancer Research, Tokyo 135-8550, Japan*
[i] *Department of Applied Chemistry Graduate School of Engineering Osaka University, Osaka 565-0871, Japan*

ARTICLE INFO

Article history:
Received 4 February 2024
Revised 6 May 2024
Accepted 21 May 2024
Available online 25 May 2024

Keywords:
3D culture
Heparin
Collagen
Ex vivo drug-screening model
Cancer microenvironment model

ABSTRACT

The development of high-throughput anticancer drug screening methods using patient-derived cancer cell (PDC) lines that maintain their original characteristics in an *in vitro* three-dimensional (3D) culture system poses a significant challenge to achieving personalized cancer medicine. Because stromal tissue plays a critical role in the composition and maintenance of the cancer microenvironment, *in vitro* 3D-culture using reconstructed stromal tissues has attracted considerable attention. Here, a simple and unique *in vitro* 3D-culture method using heparin and collagen together with fibroblasts and endothelial cells to fabricate vascularized 3D-stromal tissues for *in vitro* culture of PDCs is reported. Whereas co-treatment with bevacizumab, a monoclonal antibody against vascular endothelial growth factor, and 5-fluorouracil significantly reduced the survival rate of 3D-cultured PDCs to 30%, separate addition of each drug did not induce comparable strong cytotoxicity, suggesting the possibility of evaluating the combined effect of anticancer drugs and angiogenesis inhibitors. Surprisingly, drug evaluation using eight PDC lines with the

Abbreviations: 2D, Two-dimensional; 3D, Three-dimensional; 5-FU, 5-Fluorouracil; ATP, Adenosine triphosphate; Afb, Afatinib; Bmab, Bevacizumab; CAViTs, Cell-assembled viscous tissue by sedimentation; CD31, Platelet endothelial cell adhesion molecule; CDDP, Cisplatin; CEA/CD66e, Carcinoembryonic antigen; CV, Capillary morphogenesis vessel; Cmab, Cetuximab; DMEM, Dulbecco's Modified Eagle's Medium; ECM, Extracellular matrix; EDTA, Ethylenediaminetetraacetic acid disodium; ELISA, Enzyme-linked immunosorbent assay; EMT, Epithelial-mesenchymal transition; EpCAM, Epithelial cell adhesion molecule; FBS, Fetal bovine serum; FITC, Fluorescein isothiocyanate; GFP, Green fluorescent protein; HE, Hematoxylin and eosin; HGF, Hepatocyte growth factor; HUVEC, Human umbilical vein endothelial cell; IHC, Immunohistochemistry; L-OHP, Oxaliplatin; LbL, Layer-by-layer; MET, MET proto-oncogene, receptor tyrosine kinase; MMP1, Matrix metalloproteinase-1; MTS, 3-(4,5-Dimethylthiazol-2-yl)-5-(3-carboxymethoxyphenyl)-2-(4-sulfophenyl)-2H-tetrazolium; NBT/BCIP, Nitro blue tetrazolium/5-bromo-4-chloro-3-indolyl phosphate; NHDF, Normal human dermal fibroblast; OSIM, Osimertinib; P/S, Penicillin/streptomycin; PBS, Phosphate-buffered saline; PDC, Patient-derived cancer cell; PDO, Patient-derived cancer organoid; PDX, Patient-derived xenograft; RFP, Red fluorescent protein; RT, Room temperature; TGF-β, Transforming growth factor-β; Tris–HCl, Tris(hydroxymethyl)aminomethane hydrochloride; VEGF, Vascular endothelial growth factor; rRNA, Ribosomal RNA.

* Corresponding author at: Business Development Division, Technical Research Institute, TOPPAN Holdings Inc. 4-3-2 Takanodai-minami, Sugito, Saitama 345-8508, Japan.
** Corresponding author at: Division of Experimental Chemotherapy, Cancer Chemotherapy Center, Japanese Foundation for Cancer Research, Tokyo 135-8550, Japan.
*** Corresponding author at: Department of Applied Chemistry, Graduate School of Engineering, Osaka University, 2-1 Yamadaoka, Suita, Osaka 565-0871, Japan.
E-mail addresses: shiro.kitano@toppan.co.jp (S. Kitano), ryohei.katayama@jfcr.or.jp (R. Katayama), m-matsusaki@chem.eng.osaka-u.ac.jp (M. Matsusaki).
[1] These authors contributed equally.

https://doi.org/10.1016/j.actbio.2024.05.037

3D-culture method resulted in a drug efficacy concordance rate of 75% with clinical outcomes. The model is expected to be applicable to *in vitro* throughput drug screening for the development of personalized cancer medicine.

Statement of significance

To replicate the cancer microenvironment, we constructed a cancer-stromal tissue model in which cancer cells are placed above and inside stromal tissue with vascular network structures derived from vascular endothelial cells in fibroblast tissue using CAViTs method. Using this method, we were able to reproduce the invasion and metastasis processes of cancer cells observed *in vivo*. Using patient-derived cancer cells, we assessed the possibility of evaluating the combined effect with an angiogenesis inhibitor.

Further, primary cancer cells also grew on the stromal tissues with the normal medium. These data suggest that the model may be useful for new *in vitro* drug screening and personalized cancer medicine.

1. Introduction

Previously, the drug research and development process consisted of creating a drug compound, conducting preclinical and clinical studies, and obtaining approval to market the drug after regulatory reviews. This process is typically associated with an extremely low success rate—approximately 1 in 20,000 to 30,000 [1]—especially for anticancer drugs, which have the lowest success rate among all pharmaceutical compounds, at 3 % [2]. One of the reasons for this low success rate is that xenografts, which are frequently used in preclinical studies, have a low correlation with clinical results [3,4]. In recent years, the use of patient derived xenografts (PDXs), in which patient cancer tissue that does not include a cancer cell line is implanted into experimental animal models, has increased, and the results reportedly correlate well with clinical findings [5]. However, in drug development, PDXs are not yet widely used to assess drug efficacy or for pharmacological evaluation procedures due to marked variations in successful implantation rates (25–75 %), extremely high cost, low throughput, and difficulty in evaluating immunological agents due to species differences [6].

Kurzrock *et al.* demonstrated that treatment with molecularly targeted drugs that match a patient's genetic mutation profile is associated with improved therapeutic outcomes [7]. However, even when active mutations are identified in comprehensive genomic profiling studies, only approximately 10 % of patients are subsequently treated. This is because the types and populations of active gene mutations vary markedly among patients and because the evaluation of appropriate therapeutic drug combinations for these patients is very time consuming. For example, the number of combinations of two drugs from 20 candidate compounds is 190, and the number of combinations of three drugs is extremely large, at 1140.

Recent studies have highlighted the importance of considering the cancer microenvironment in drug development [8–12]. In particular, co-culture of cancer cells with stromal tissues and construction of cancer microenvironments consisting of complex structures and functions are necessary to assess factors such as cancer cell proliferation, differentiation, migration, metastasis, and acquisition of drug resistance, because stromal tissues contribute significantly to these characteristics [13–18]. Stromal cells include cancer-associated endothelial cells, cancer-associated fibroblasts, cancer-associated macrophages, and immune cells, among others. The complexity of interactions between each stromal cell and cancer cell type can induce the formation of cancer microenvironment–specific characteristics, such as abnormal vascular network structures and hypoxia. In order to establish a suitable cancer microenvironment, it is desirable to use a co-culture system in which the position, morphology, and number of each fraction can be controlled within the tissue.

Three-dimensional (3D) cell culture techniques, such as the use of spheroids or organoids, are reportedly superior methods for evaluating anticancer drugs [19,20]. However, because spheroids can spontaneously form cell clusters, it is difficult to control the position of cancer cells and stromal cells, such as fibroblasts, in the same tissue during co-culture. Organoid technology is predicted to become an important tool for embryological research [21–24] and cancer precision medicine [25], but according to a meta-analysis of observational studies, the clinical utility of organoid-based drug screening has not been sufficiently proven [26]. Only 30 % of studies in the meta-analysis showed statistically significant correlations between screening results and clinical response [26]. Furthermore, growth factors and other supplements in culture media could potentially affect drug efficacy [27,28]. Although cell sheets can be stacked one atop another to create 3D tissue layers, the methodology is complex [29]. A global challenge in co-culture systems is that no established methods are available that enable selective evaluation of only the cancer cell fraction in tissues composed of multiple cell types [30].

We previously described a cancer model using the layer-by-layer (LbL) method, in which alternate layers of fibronectin and gelatin are used to coat the fibroblast surface [31–34]. The LbL method is characterized by the assembly of cells and tissues through interactions involving the functional properties of the cell membrane with natural polysaccharides and the extracellular matrix (ECM) [35]. Cell signaling events in the tissue microenvironments of living organisms are mediated by proteins, glycosaminoglycans, and glycoproteins on the cell membrane [36–40], all of which play important roles in cell adhesion, proliferation, differentiation, and other functions. Thus, the LbL method is a potentially useful 3D cell culture technique that can potentially mimic the cancer microenvironment. However, due to the many centrifugation steps (20 times for 20 layers) required to alternately coat cells with different proteins, the application of the method is associated with considerable cell damage and cell volume loss (>70 %) [41].

To overcome the limitations of the LbL method, we recently developed a simple and unique tissue engineering technique that we refer to as the cell assembled viscous tissue by sedimentation (CAViTs) method, which can be used to assess toxicity affecting the vascular structure of the liver [42]. This innovative approach enables the rapid organization of cells using collagen, the primary ECM component involved in cell adhesion, and heparin, which interacts with many growth factors on cell surfaces. The LbL method requires 20 centrifugation steps and a processing time of >20 min,

resulting in a final cell yield of approximately ≤30 %. By contrast, the CAViTs method requires only one centrifugation step, which minimizes the processing time to only a few minutes, and cell yield rates of >90 % can be obtained [42].

In this study, we applied the CAViTs technology to cancer microenvironment models and evaluated the feasibility of the models as drug screening tools. First, we improved the original CAViTs protocol to mimic cancer cell morphology by selecting the best ECM component to construct stromal tissues. Second, the combined effects of anticancer drugs and angiogenesis inhibitors, which typically cannot be evaluated using *in vitro* drug screening models due to the lack of a vascular network, were evaluated using actual patient-derived cancer cells (PDCs). Furthermore, the clinical extrapolation results were evaluated using our vascularized cancer stromal tissue models because their higher biomimetic properties might allow for more accurate assessments of drug efficacy. Third, the feasibility of co-culturing cancer stromal tissue models with primary cancer cells without external growth factors was evaluated, as primary cancer cells should grow well due to the paracrine effect of growth factors released from the stromal tissues.

2. Materials and methods

2.1. Polyelectrolytes, the ECMs, and solvent

The polyelectrolytes used in the study included dextran sulfate (D8906, Merck Millipore Corp.), polystyrene sulfonic acid (516-85751, Fujifilm Corp.), and polyacrylic acid (165-18571, Fujifilm Corp.). Heparin (H3149, Merck Millipore Corp.), chondroitin sulfate A (C6737, Merck Millipore Corp.), chondroitin sulfate C (034-08801, Fujifilm Corp.), dermatan sulfate (1171455, Fujifilm Corp.), and hyaluronic acid (087-04511, Fujifilm Corp.) were used as the glycosaminoglycan ECM components. The cell adhesive ECM components used in the study included collagen I (ASC-1-100-100, Fujifilm Corp.), laminin (120-05751, Fujifilm Corp.), and fibronectin (F1141, Merck Millipore Corp.). Tris–HCl buffer (pH 7.4) (Tris) (T7693, Merck Millipore Corp.) was used as a solvent.

2.2. Reagents and antibodies

The anticancer agents used in the study included 5-fluorouracil (5-FU) (064–01403, Fujifilm Corp.), oxaliplatin (L-OHP) (Nippon Kayaku Corp., Tokyo, Japan), cetuximab (Cmab) (Merck Biopharma Corp.), irinotecan (091–06651, Fujifilm Corp.), SN-38 (S589950, Fujifilm Corp.), and bevacizumab (Bmab) (Chugai Pharmaceutical Corp.). Antibodies included anti–vascular endothelial growth factor (VEGF) monoclonal antibody (MAB293, R&D Systems), Ep-CAM monoclonal antibody (#2929S, Cell Signaling Technology Corp.), cytokeratin 7 monoclonal antibody (ab181598, Abcam PLC.), Pan Cytokeratin Monoclonal Antibody (MA5-13156, Invitrogen.), carcinoembryonic antigen (CEA)/CD66e monoclonal antibody (#2383, Cell Signaling Technology Corp.), Non-phospho (Active) β-Catenin(#8814, Cell Signaling Technology Corp.), CK8/18 monoclonal antibody (M3652, Agilent Corp.), platelet endothelial cell adhesion molecule (CD31) monoclonal antibody (M0823, Agilent Corp.), and anti–hepatocyte growth factor (HGF) antibody (MAB294, R&D Systems Corp.). Secondary antibodies included goat anti-mouse IgG (H+L) highly cross-adsorbed secondary antibody, Alexa Fluor 488 (A11001, Thermo Fisher Scientific Corp.), goat anti-mouse IgG (H+L) highly cross-adsorbed secondary antibody, Alexa Fluor 594 (A11032, Thermo Fisher Scientific Corp.), and goat anti-mouse IgG (H+L) highly cross-adsorbed secondary antibody, Alexa Fluor 647 (A21236, Thermo Fisher Scientific Corp.). Trypsin-EDTA (0.25 %), TrypLE Express (12605036, Thermo Fisher Scientific Corp.), and Tumor Dissociation kit (#130-095-929, Miltenyi Biotec B.V. & Corp. KG) were used as cell dispersion reagents. Fluorescent labeling reagents included PKH26 Red Fluorescent Cell Linker kit (PKH26GL, Merck Millipore Corp.), PKH67 Green Fluorescent Cell Linker kit (PKH67GL, Merck Millipore Corp.), Cell Tracker Green (C7025, Thermo Fisher Scientific Corp.), and Cell Tracker Red (C34552, Thermo Fisher Scientific Corp.).

2.3. Cell lines and cell cultures

Cells comprising the human 3D stromal tissue model included normal human dermal fibroblasts (NHDFs) (CC-2509, Lonza Group Ltd.), human umbilical vein endothelial cells (HUVECs) (CC-2517A, Lonza Group Ltd.), green fluorescent protein (GFP)-transduced HUVECs (GFP-HUVECs) (cAP-0001GFP, Angio-Proteomie Corp.), or red fluorescent protein (RFP)-transduced HUVECs (RFP-HUVECs) (cAP-0001RFP, Angio-Proteomie Corp.), NHDFs were pre-cultured in Dulbecco's Modified Eagle's Medium (DMEM) (043-30085, Fujifilm Corp.) containing 10 % fetal bovine serum (FBS) (10437028, Thermo Fisher Scientific Corp.) and 1 % penicillin/streptomycin (P/S) at 37 °C in a 5 % CO_2 incubator. HUVECs, GFP-HUVECs, and RFP-HUVECs were pre-cultured using EGM™-2 MV Bullet kit™ (CC3202, Lonza Group Ltd.) medium in a CO_2 incubator (37 °C, 5 %).

The human-derived cancer cells used in the experiments consisted of colorectal adenocarcinoma cell lines HT29 (HTB-38™, American Type Culture Collection [ATCC]), HCT116 (CCL-247, ATCC) HT115 (85061104, European Collection of Authenticated Cell Cultures), gastric cancer cell line NCI-N87 (CRL-5822, ATCC), and non-small cell lung cancer cell line NCI-H1975 (CRL-5908, ATCC). HT29 and HCT116 cells were pre-cultured in McCoy's 5A medium (12-168F, Lonza Group Ltd.) containing 10 % FBS and 1 % P/S in a CO_2 incubator (37 °C, 5 %). HT115 cells were pre-cultured in DMEM containing 15 % FBS and 1 % P/S in a CO_2 incubator (37 °C, 5 %). NCI-N87 and NCI-H1975 cells were pre-cultured in RPMI-1640 medium (A104910, Thermo Fisher Scientific Corp.) containing 10 % FBS and 1 % P/S in a CO_2 incubator (37 °C, 5 %).

2.4. Patient selection and establishment of PDCs

Colorectal cancer surgical specimens were collected from patients who underwent surgery for primary and metastatic colorectal tumors. The patients submitted written informed consent for genetic and biological analyses, which were performed in accordance with the protocols approved by the Institutional Review Board of the Japanese Foundation for Cancer Research (JFCR) (#2013-1093).

Several pieces of the surgically resected tumors were immediately transferred into ice-cold culture medium and enzymatically processed to establish PDC lines, as previously reported [43]. PDCs established at the JFCR from surgically resected colorectal cancers were designated JC-XXX-(nth time)-(tumor site). For example, JC-119-1-TR and JC-119-2-Liv indicate PDCs from patient #119 and first-time tumor from the rectum (TR) and second-time tumor from the liver as a metastatic site.

JC-039-2-Liv, JC-054-3-Liv, JC-063-1-TS, JC-072-2-Liv, JC-075-1-TS, JC-075-2-Liv, JC-119-1-TR, JC-119-2-Liv, JC-143-1, JC-004, JC-247, JC-278 and JC-406 cells were pre-cultured in 50 % StemPro hESC SFM (A1000701, Thermo Fisher Scientific Corp.), that is, DMEM/F-12 containing GlutaMAX (10565018, Thermo Fisher Scientific Corp.) supplemented with 0.5 % StemPro hESC supplement, 1.3 % bovine serum albumin (A10008-011, Thermo Fisher Scientific Corp.), 6.4 ng/mL fibroblast growth factor–basic (100-18B, Peprotech Corp.), 0.08 mM 2-mercaptoethanol (21985-023, Thermo Fisher Scientific Corp.), 8 μM Y-27632 (Y-5301, LC Laboratories Corp.), and 1 % antibiotic-antimycotic solution (15240062, Thermo Fisher Scientific Corp.) in a CO_2 incubator (37 °C, 5 %).

2.5. Observation of viscous bodies obtained by CAViTs

First, 1.0×10^7 NHDFs were suspended in a mixture of 1 mg/mL FITC-modified heparin/50 mM Tris–HCl (pH 7.4) solution and 1 mg/mL collagen/acetic acid (pH 3.7) solution, added to a Petri dish, and centrifuged at 1000 × *g* for 5 min. Any remaining viscous material was observed by fluorescence and polarized light microscopy.

2.6. Evaluation of cohesion effects by CAViTs

First, 1.0×10^6 NHDFs were incubated in a mixture of 0.05 mg/mL heparin/50 mM Tris–HCl (pH 7.4) solution and 0.05 mg/mL collagen/acetic acid (pH 3.7) solution, 0.05 mg/mL heparin/50 mM Tris–HCl (pH 7.4) solution only, 0.05 mg/mL collagen/acetic acid (pH 3.7) solution only, or 50 mM Tris–HCl (pH 7.4) solution only and then centrifuged at 700 × *g* for 5 min. The produced viscous material was resuspended in 1.5 mL of 10 % FBS– and 1 % P/S–containing DMEM (culture medium), and an aliquot was placed on a Petri dish and observed under an inverted phase-contrast microscope (BZ-X710, KEYENCE Corp). The number of clusters and cell viability were measured using a cell counter (Vi-CELL BL, Beckman Coulter Inc.).

2.7. Construction of 3D stromal tissue model using CAViTs

2.7.1. NHDF single culture

First, 3.5×10^6 NHDFs were suspended in a mixture of 250 µL of 0.2 mg/mL or 0.1 mg/mL polyelectrolyte/50 mM Tris–HCl (pH 7.4) solution and 250 µL of 0.1 mg/mL or 0.05 mg/mL ECM/acetic acid (pH 3.7) solution at room temperature (RT) and centrifuged at 400 × *g* for 1 min to obtain viscous material. After suspending the obtained viscous material in culture medium, the suspension was seeded in a 24-well cell culture insert (#3470, Corning Inc.) and centrifuged at 400 × *g* for 1 min at RT. Culture medium was then added to the 24-well cell culture inserts and incubated in a CO_2 incubator (37 °C, 5 %) for 24 h.

2.7.2. NHDF and HUVEC co-culture

Viscous material was obtained by centrifuging 2.0×10^6 NHDFs and 3.0×10^4 HUVECs in a mixture of 300 µL of heparin/50 mM Tris–HCl (pH 7.4) solution and 0.05 mg/mL collagen/acetic acid (pH 3.7) solution at 400 × *g* for 1 min at RT. After suspending the obtained viscous material in culture medium, the suspension was seeded in 24-well cell culture inserts and centrifuged at 400 × *g* for 1 min at RT. Culture medium was then added to the 24-well cell culture inserts and incubated in a CO_2 incubator (37 °C, 5 %) for 96 h.

2.7.3. Five-layer culture

NHDFs (0.6×10^6 cells) pre-fluorescently stained with Cell Tracker Green were suspended in 150 µL of 0.2 mg/mL heparin/50 mM Tris–HCl buffer (pH 7.4) and 150 µL of 0.2 mg/mL collagen/acetic acid solution (pH 3.7). The resulting suspension was then seeded in a 24-well cell culture insert and centrifuged at 400 × *g* for 1 min at RT to form the first cell layer. Using the same technique, a second cell layer was formed on top of the first cell layer using NHDFs (0.6×10^6 cells) pre-fluorescently stained with Cell Tracker Red. A third cell layer was then formed on top of the second cell layer using NHDFs (0.6×10^6 cells) pre-stained with Cell Tracker Green using the same method. A fourth cell layer was formed on top of the third cell layer using NHDFs (0.6×10^6 cells) pre-stained with Cell Tracker Red. A fifth cell layer was formed on top of the fourth cell layer using NHDFs (0.6×10^6 cells) pre-fluorescently stained with Cell Tracker Green. Finally, culture medium was added to the cell culture inserts and incubated in a CO_2 incubator (37 °C, 5 % CO_2) for 24 h.

2.7.4. Cancer formation on top of stromal tissue

First, 2.0×10^6 NHDFs and 3.0×10^4 HUVECs co-cultured with 3D stromal tissues were prepared as described in Section 2.7.2 (referred to as the CAViTs method) in 24- or 96-well cell culture inserts (#3470 or #7369, Corning Inc.) and cultured for 24 h. Next, 2.0×10^4 cancer cells were suspended in culture medium, and the suspensions were seeded in the 24-well cell culture inserts and incubated in a CO_2 incubator (37 °C, 5 %) for 96 h.

2.7.5. Cancer in stromal tissue (sandwich)

First, 1.0×10^6 NHDFs and 1.5×10^4 HUVECs co-cultured with 3D stromal tissues were prepared using the CAViTs method in 24-well cell culture inserts and cultured for 24 h. Next, 2.0×10^4 cancer cells were suspended in culture medium and then seeded in the 24-well cell culture inserts and incubated in a CO_2 incubator (37 °C, 5 %) for 1 h. Finally, 1.0×10^6 NHDFs and 1.5×10^4 HUVECs co-cultured with 3D stromal tissues were prepared using the CAViTs method in 24-well cell culture inserts and cultured for 96 h.

2.8. Cell counting and cell layer density evaluation

NHDF single cultures were prepared using the CAViTs method, fixed in 10 % formalin (060-03845, Fujifilm Corp.), immersed in 70 % ethanol (059-07895, Fujifilm Corp.), and paraffin-embedded sections were prepared using established methods. The sections were then stained with hematoxylin and eosin (HE). The maximum number of cell layers and the thickness (µm) of the area with the maximum number of cell layers were then measured for each section. From the maximum cell layer count and thickness measurements, the number of cell layers per 10-µm thickness (i.e., cell layer density) was calculated.

2.9. Evaluation of self-assembled vascular network formation and inhibition

To evaluate self-assembled vascular network formation, NHDFs and HUVECs co-cultured with 3D stromal tissues were prepared using the CAViTs method in 24-well cell culture inserts and cultured for 1, 4, and 8 days.

To evaluate self-assembled vascular network inhibition, NHDFs and HUVECs co-cultured with 3D stromal tissues were prepared using the CAViTs method in 24-well cell culture inserts and cultured for 24 h. Anti-HGF (10 µg/mL) and anti-VEGF bevacizumab (10 µg/mL) were added and incubated in a CO_2 incubator (37 °C, 5 %) for 72 h.

After culture, the cells in each evaluation were washed twice with PBS and fixed with 10 % formalin, and the vascular network structure was observed using anti-CD31 primary antibody and secondary antibody on a high-content confocal microscope analysis system. Paraffin-embedded sections were prepared according to established methods. Immunohistochemistry (IHC) analysis of the sections was performed using the anti-CD31 antibody.

2.10. Evaluation of 3D stromal tissue model viability

Three-dimensional stromal tissues prepared using the CAViTs method with either NHDFs alone or NHDFs and HUVECs were cultured for 8 days before being dispersed with cell dispersion reagent and subjected to viability assessment using an automated cell counter (Countess® II FL, Thermo Fisher Scientific Corp.).

2.11. Drug efficiency evaluation

2.11.1. Two-dimensional cultures

First, 2.0×10^4 cancer cells were suspended in the medium used for pre-culture. The resulting suspensions were seeded in 24-

well cell culture inserts or black 96-well plates with clear bottoms (Greiner Bio-one GmbH, 655090) and incubated in a CO_2 incubator (37 °C, 5 %) for 24 h. Anticancer drugs or antibodies were then added, and the cells were cultured in a CO_2 incubator (37 °C, 5 %) for at least 72 h. The effect of the drugs was then evaluated by counting the cancer cells. The number of cancer cells was measured using an automated cell counter or MTS (3-[4,5-dimethylthiazol-2-yl]-5-[3-carboxymethoxyphenyl]-2-[4-sulfophenyl]-2H-tetrazolium) or ATP (adenosine triphosphate) assay kits (G5430 or G9242, Promega Corp.).

2.11.2. Spheroid cultures

First, 2.0×10^4 cancer cells were suspended in DMEM containing 10 % FBS and 1 % P/S. The resulting suspensions were seeded in Perfecta3D® Hanging Drop Plates (NT-HDP1096, 3D Biomatrix Inc.) and incubated in a CO_2 incubator (37 °C, 5 %) for 96 h. Anticancer drugs or antibodies were then added, and the cells were cultured in a CO_2 incubator (37 °C, 5 %) for at least 72 h. The effect of the drugs was evaluated by counting the cancer cells using an automated cell counter after the addition of cell dispersion reagent.

2.11.3. CAViTs

Cancer co-culture models were prepared using 24-well or 96-well cell culture inserts. Anticancer drugs or antibodies were added to cells cultured in a CO_2 incubator (37 °C, 5 %) for at least 72 h. The effect of the drugs was then evaluated by counting the cancer cells. To count cancer cells, 3D tissues prepared using the CAViTs method were first dispersed with a cell dispersion reagent, and then the number of cancer cells, which had been fluorescently labeled at the time of CAViTs 3D tissue preparation, was determined using an automated cell counter. Alternatively, the efficacy of the drugs was evaluated by calculating the confluence of cultured cancer cells. The area occupied by cancer cells was measured using a high-content confocal microscope analysis system after fluorescent immunostaining of either EpCAM or CK8/18 expressed on the cell surface.

2.12. Evaluation and validation of drug efficacy in PDCs from eight patients

After the cancer co-culture model was prepared in 24-well cell culture inserts using PDCs from eight patients, anticancer drugs were added, and the cells were cultured in a CO_2 incubator (37 °C, 5 %) for at least 72 h. The effect of each drug was then evaluated by counting the cancer cells or calculating the area occupied by cancer cells after staining for EpCAM or CK8/18.

Drug efficacy against PDCs was evaluated using the same drugs and regimens originally used in treatment of the patients. JC-039-2-Liv received 5-FU+L-OHP; JC-054-3-Liv received 5-FU+L-OHP+Bmab; JC-063-1-TS, JC-072-2-Liv, JC-075-1-TS, and JC-075-2-Liv received 5-FU+L-OHP+Cmab; and JC-119-1-TR and JC-119-2-Liv received 5-FU+L-OHP+SN-38+Bmab.

Drug concentration ratios were kept constant and based on mFOLFOX6 and FOLFOXIRI regimens. Rapid and continuous intravenous infusions were not distinguished but added together. Because some doses were expressed in mg/m^2 and others in mg/kg, the ratios were determined using 165 cm/60 kg. The maximum concentrations of the anticancer drugs were set at 1000 μM for 5-FU, 10 μM for L-OHP and SN-38, 8.3 μg/mL for Bmab, and 18.5 μg/mL for Cmab.

Drug efficacy was judged based on the percentage of cancer cells remaining relative to control samples at the specific concentration tested. A 5-FU concentration of 250 μM was determined as the criterion concentration, and 80 % was selected as the sensitive/non-sensitive threshold; that is, the PDCs were judged as non-sensitive to the tested set of drugs when the residuals were $>$80 % at that concentration or below. In contrast, in the case of residual values of $\leq$80 %, the PDCs were judged as sensitive.

2.13. Primary cancer cell culture in 3D stromal tissue generated using CAViTs

2.13.1. Preparation of primary cancer cells

Primary cancer cells were obtained from surgically removed tumor tissue that had been cut into small pieces, treated with collagenase/dispase (10269638001, F. Hoffmann-La Roche Ltd.), and fractionated using a filter with a pore size of 100 μm.

2.13.2. Effect of culture method

Primary cancer cells that had been fluorescently labeled with PKH26 Red Fluorescent Cell Linker kit or PKH67 Green Fluorescent Cell Linker kit were 2D cultured or cultured with/without capillary morphogenesis vessels in 3D culture using a stromal tissue model generated using the CAViTs method. Alternatively, primary cancer cells were cultured on a HUVEC feeder. On days 5 and 13, cancer cells were observed under a microscope (BZ-X700, KEYENCE Corp.), and the area occupied by cancer cells was calculated.

2.13.3. Effect of the number of stromal cell layers

Primary cancer cells were cultured on 3D stromal tissue models comprising 1, 5, 10, or 20 stromal cell layers (1.0×10^5 cells/layer) prepared using the CAViTs method. After 14 days of culture, the cells were dispersed, washed twice with PBS, and fixed with 10 % formalin. After staining with fluorescence-labeled anti-EpCAM antibody, the cells were counted using an automated cell counter, and the proliferation rate (measured value/number of cells seeded $\times$ 100) was calculated.

2.13.4. Effect of HUVEC content

Primary cancer cells were cultured on 3D stromal tissue models with a HUVEC content of 0, 0.5, 1.5, or 5.0 % prepared using the CAViTs method. After 14 days of culture, the cells were dispersed, washed twice with PBS, and fixed with 10 % formalin. After staining with fluorescently labeled anti-EpCAM antibody, the cells were counted using an automated cell counter, and the growth rate (measured value/number of cells seeded $\times$ 100) was calculated.

2.14. IHC analysis

2.14.1. HE staining

For HE staining, cultured tissue was washed twice with PBS and fixed with 10 % formalin overnight at 4 °C. Tissue sections were deparaffinized with xylene, rehydrated through an ethanol series, and rinsed in running tap water for 5 min. The sections were then treated with hematoxylin (H3136, Merck Millipore Corp.), rinsed in running tap water, and treated with eosin alcohol (HT110116, Merck Millipore Corp.). The sections were then dehydrated through an ethanol series and xylene and mounted with malinol (10781, Muto Pure Chemicals Corp.).

2.14.2. Cytokeratin 7

For IHC, cultured tissue was washed twice with PBS and then fixed with 10 % formalin overnight at 4 °C. Tissue sections were deparaffinized with xylene and rehydrated through an ethanol series and TBS (935B, Merck Millipore Corp.). Antigen retrieval was performed by microwave treatment with EDTA buffer at pH 9.0. Endogenous peroxidase activity was blocked by treatment with 0.3 % H_2O_2 in methanol for 30 min, followed by incubation with Protein Block (GB-01, GenoStaff1 Corp.) and an avidin/biotin blocking kit (SP-2001, Vector Laboratories Inc.). The sections were then incubated with anti–cytokeratin 7 rabbit monoclonal antibody (Ab181598, Abcam PLC.) at 4 °C overnight. Next, the sections were incubated with biotin-conjugated goat anti-rabbit Ig

(E0432, Agilent Corp.) for 30 min at RT, followed by the addition of peroxidase-conjugated streptavidin (525-33251, Fujifilm Corp.) and incubation for 5 min. Peroxidase activity was visualized using diaminobenzidine (D12384, Merck Millipore Corp.). The sections were counterstained with Mayer's hematoxylin (30002, Muto Pure Chemicals Corp.), dehydrated, and then mounted with malinol.

2.14.3. CEA & CD31

For the first IHC staining procedure, cultured tissue was washed twice with PBS and then fixed with 10 % formalin overnight at 4 °C. Tissue sections were deparaffinized with xylene and rehydrated through an ethanol series and TBS. Antigen retrieval was performed by microwave treatment in citrate buffer at pH 6.0. Endogenous peroxidase activity was blocked by treatment with 0.3 % H_2O_2 in methanol for 30 min, followed by incubation with Protein Block and an avidin/biotin blocking kit. The sections were incubated with anti-CD31 mouse monoclonal antibody at 4 °C overnight, followed by incubation with biotin-conjugated rabbit anti-mouse IgG for 30 min at RT and the addition of alkaline phosphatase–conjugated streptavidin and incubation for 10 min. Alkaline phosphatase activity was visualized using NBT/BCIP (11681451001, Merck Millipore Corp.), followed by washing with PBS.

For the second IHC staining procedure, antibody dissociation was performed by heat treatment with citrate buffer at pH 6.0. The sections were then incubated with Protein Block and an avidin/biotin blocking kit and incubated with anti-CEA mouse monoclonal antibody (#2383, Cell Signaling Technology Corp.) at 4 °C overnight. The sections were then incubated with biotin-conjugated rabbit anti-mouse IgG for 30 min at RT, followed by the addition of peroxidase-conjugated streptavidin and incubation for 5 min. Peroxidase activity was visualized using diaminobenzidine, and the sections were mounted with CC/Mount (K002, Diagnostic BioSystems Inc.).

2.15. Microarray analysis

2.15.1. Sample preparation

Three-dimensional tissues were prepared in 24-well cell culture inserts with vascular-free NHDFs only. The tissues were dissolved in QIAzol Lysis Reagent (79306, QIAGEN N.V.) and stored at −80 °C. The steps from RNA extraction to microarray analysis described below were outsourced to the Chemicals Evaluation and Research Institute.

2.15.2. Total RNA extraction

A total of 100 µL of cell disruption fluid was added to QIAzol Lysis Reagent to reach 700 µL, and the cells were further disrupted by centrifugation on a QIAshredder column (79656, Qiagen N.V.). Thereafter, 20 % (vol) of the filtrate was added to chloroform, mixed thoroughly, and centrifuged. After the supernatant was removed, a 1.5-fold volume of 100 % ethanol was added to precipitate total RNA, which was purified using a miRNeasy Micro kit (217084, Qiagen N.V.). Finally, 20 µL of nuclease-free water was added to elute the total RNA. The total RNA extracted using the miRNeasy Micro kit was stored at −80 °C.

2.15.3. Measurement of total RNA concentration and RNA quality testing (Bioanalyzer analysis)

To calculate RNA concentration and purity, the absorbance of the total RNA solution was measured using an Ultra-trace spectrophotometer (NanoDrop™ One, Thermo Fisher Scientific Corp.) at 230, 260, and 280 nm (A260/280 and A260/230). The concentration required for microarray analysis was ≥4 ng/µL, and good purity was defined as A260/280 ≥1.8 and A260/230 ≥1.5. When the concentration of total RNA solution (stock solution) was ≥100 ng/µL, a portion of the total RNA solution (stock solution) was aliquoted and then diluted to 100 ng/µL for subsequent analysis.

For bioanalysis, 1 µL of total RNA solution was aliquoted and diluted 2-fold by adding nuclease-free water. The sample was then placed on a microchip prepared using an RNA6000 Nano kit (Agilent Corp.), and electrophoresis was performed by setting the microchip on a 2100 Bioanalyzer (Agilent Corp.). From the electrophoresis results, the RNA Integrity Number (RIN) and rRNA ratio (28S/18S), which are indicators of RNA degradation, were calculated. rRNA quality was considered good when the RIN was ≥7.0.

2.15.4. Microarray

An Agilent SurePrint G3 Human GE v3 8×60 K Microarray (design ID: 072363, Agilent Technologies Inc.,) was used for this analysis, and the microarray chips were scanned using an Agilent DNA microarray scanner (Agilent Technologies Inc.). Intensity values for each scanned feature were quantified using Agilent Feature Extraction software, version 10.7.1.1. Normalization was performed with Agilent GeneSpring, version 14.5 (per chip: normalization to 75th percentile shift). Altered transcripts were quantified using the comparative method. Raw and normalized microarray data are available in the Gene Expression Omnibus database (accession number GSE248026).

2.16. ELISA

Quantitation of secreted VEGFA and HGF in a layered 3D tissue medium was performed using a Quantikine human VEGF ELISA kit (DVE00, R&D Systems Corp.) and a Quantikine human HGF ELISA kit (DHG00B, R&D Systems Corp.), according to the manufacturer's instructions.

A total of 1.3 mL of medium was harvested from the 3D tissue or 2D cell culture in 24-well inserts and then incubated for 4 days, filtered, and analyzed in duplicate. Absorbance was determined using a microplate reader (Multiskan™ FC, Thermo Fisher Scientific Corp.) set to 450 nm, with the wavelength correction set to 540 nm.

2.17. Statistical analyses

Data are expressed as mean ± SD of triplicate samples. Differences between groups were analyzed using the Student's *t*-test. A *P*-value <0.05 was considered statistically significant. Dose-responce curves were fitted and IC_{50} values were calculated using the biostatistical analysis software GraphPad Prism (GraphPad Software Inc.).

3. Results

3.1. CAViTs method

The CAViTs method is a simple 3D tissue preparation method that takes advantage of the heparin-cell aggregation effect and collagen type I cell adhesiveness that we reported previously [42]. Fig. 1a shows a schematic illustration of the tissue preparation procedure. Cells, heparin (a natural polysaccharide), and collagen type I were mixed in a Tris–HCl buffer, and the cells were induced to agglutinate by applying an external force, such as centrifugal force, to form a viscous body (Fig. 1b). The resulting viscous material was resuspended in culture medium and then dispensed into transwell permeable supports and cultured to easily obtain 3D tissues within 5 min. The presence of viscous material was confirmed under a microscope using a polarizer with orthogonal polarization and birefringence (liquid crystallinity; i.e., light passing through the viscous material that appears white; Fig. 1c).

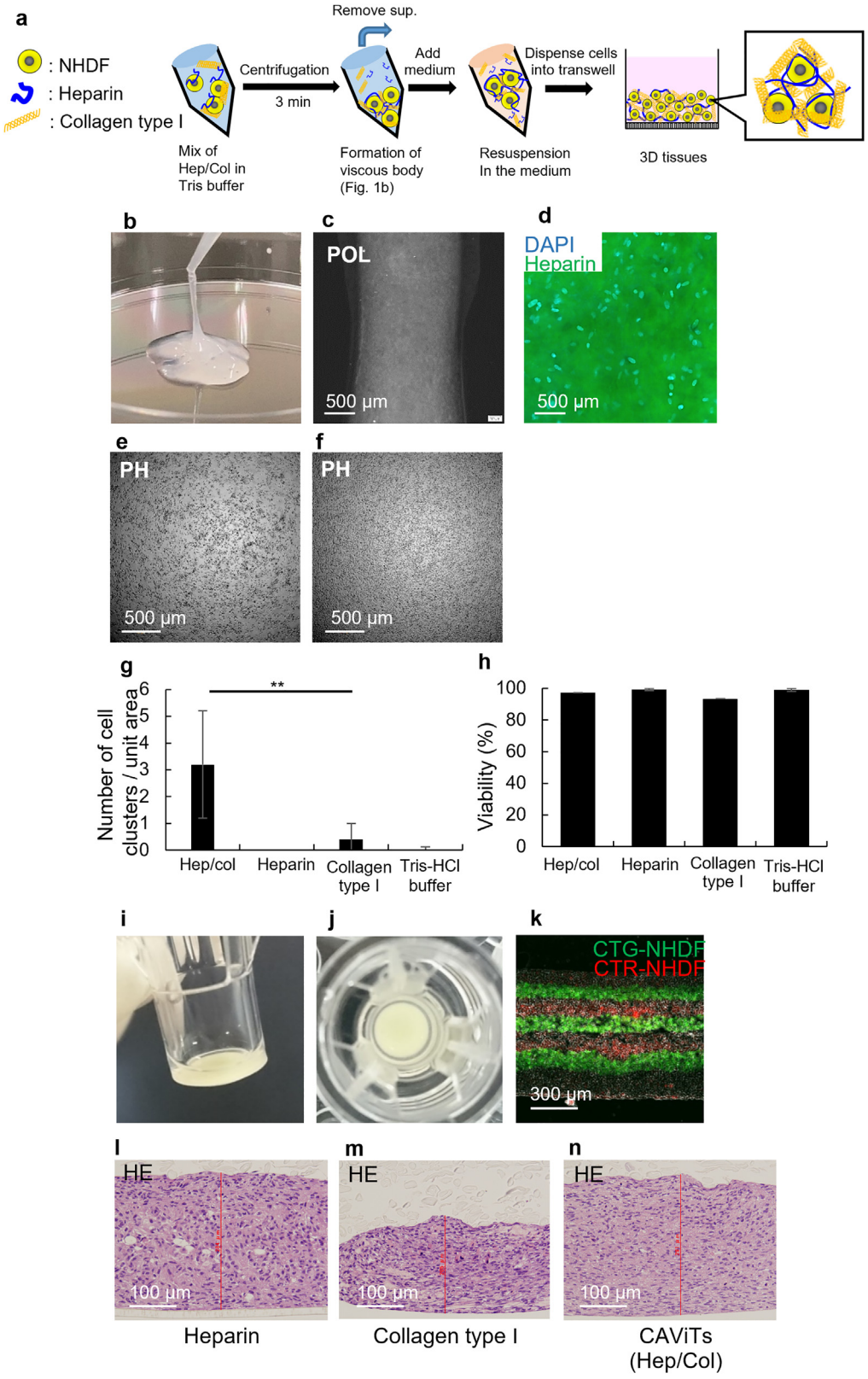

Fig. 1. Overview of the CAViTs method.
Schematic illustration of the CAViTs procedure (a). Photograph of the viscous body prepared by the CAViTs method (b). Polarized image of the resuspended viscous body in culture medium (c). Fluorescent image of the resuspended viscous body in culture medium (green: heparin, blue: DAPI) (d). Phase-contrast image of the viscous body prepared using the CAViTs method to confirm CAViTs-induced aggregation (e). Phase-contrast image using Tris–HCl buffer as a control (f). Number of cell clusters/field of view (g) and viability (%) (h) per condition. Lateral substantive image (i) and top-view image (j) of 3D tissues prepared by the CAViTs method. Cross-sectional fluorescent image (green: cell tracker green–stained NHDFs [CTG-NHDFs]), red: cell tracker red–stained NHDFs [CTR-NHDFs]) of five-layer laminated culture prepared on culture inserts using the CAViTs method (k). HE-stained images of 3D tissue prepared by each condition (l: heparin, m: collagen type I, n: CAViTs). $^{**}P<0.05$.

Table 1
Validation of the CAViTs method (comparative evaluation with materials other than heparin and collagen type 1).

		ECM (Adhesion factors)							
		None		Collagen type I		Laminin		Fibronectin	
		Thickness (μm)	Cell density (cells/ 5×10^3 μm^2)	Thickness (μm)	Cell density (cells/ 5×10^3 μm^2)	Thickness (μm)	Cell density (cells/ 5×10^3 μm^2)	Thickness (μm)	Cell density (cells/ 5×10^3 μm^2)
ECM (Glycosaminoglycans)	None	163 ± 0.92	69.5 ± 7.05	191 ± 13	83.6 ± 1.99	155 ± 4.2	72.7 ± 9.82	170 ± 3.5	84.2 ± 4.86
	Heparin	280 ± 3.4	54.9 ± 1.84	286 ± 9.7	62.1 ± 0.348	149 ± 2.4	69.6 ± 17.7	165 ± 8.2	64.8 ± 9.53
	Chondroitin sulfate A	113 ± 4.7	62.9 ± 3.98	465 ± 29	40.4 ± 4.33	196 ± 4.3	65.3 ± 5.00	105 ± 1.6	70.4 ± 5.66
	Chondroitin sulfate C	220 ± 15	56.9 ± 6.88	259 ± 6.7	94.8 ± 6.52	188 ± 4.7	61.6 ± 5.97	101 ± 2.7	67.7 ± 16.9
	Dermatan sulfate	235 ± 4.7	50.3 ± 5.92	433 ± 4.8	48.0 ± 1.61	176 ± 2.7	70.0 ± 2.39	242 ± 19	81.1 ± 3.85
	Hyaluronic acid	196 ± 3.3	49.0 ± 10.6	287 ± 3.3	72.8 ± 6.70	185 ± 7.9	73.4 ± 9.44	143 ± 1.1	65.1 ± 8.45
Polyelectrolytes	Dextran sulfate	121 ± 2.2	67.0 ± 3.55	316 ± 5.2	76.7 ± 4.11	197 ± 9.4	72.5 ± 1.39	194 ± 5.0	83.1 ± 2.15
	Polystyrene sulfonic acid	213 ± 8.1	52.6 ± 4.46	401 ± 10	49.3 ± 3.50	90.7 ± 3.1	61.0 ± 3.41	158 ± 5.8	77.5 ± 6.08
	Polyacrylic acid	232 ± 0.61	55.7 ± 0.824	201 ± 7.2	64.0 ± 5.67	172 ± 0.95	57.5 ± 3.33	161 ± 9.0	68.1 ± 5.30

Results are shown for evaluation sections of tissue constructed from cell suspensions with final concentrations of glycosaminoglycan ECM or polyelectrolytes components (listed in the first and second column of the table) and adhesion factor ECM (listed in the first and second rows of the table) of 0.1 mg/mL each. The numbers in the thickness and cell density column indicate the mean ± SD of three different points of measurement of each HE-stained section. Number of cells was measured by visually counting cell nuclei. "None" in the polyelectrolyte component condition list (first column of the table) means no polyelectrolyte. "None" in the ECM components condition list (listed in the first row of the table) means no ECM.

After resuspending the viscous material in culture medium, we confirmed that heparin was retained between the cells (Fig. 1d) and that the cells aggregated within 1 min after the CAViTs procedure was implemented (Fig. 1e). In contrast, in the control, which contained Tris–HCl buffer, few cells aggregated and remained uniformly dispersed in the Petri dish after 20 min (Fig. 1f). The number of clusters in which one or more cells aggregated in one field of view was 3.2 for the CAViTs method (i.e., heparin and collagen type I together), 0 for heparin only, 0.4 for collagen type I only, and 0 for samples lacking both heparin and collagen type I (Fig. 1g), thus confirming the roles of heparin and collagen in this aggregation effect. Cell viability after undergoing the CAViTs method was 97.2 % (±0.7), indicating that the treatment had a strong aggregation-inducing effect but did not reduce the viability of the cells (Fig. 1h).

Fig. 1k shows the evaluation of sections after 1 day of culture, in which fibroblasts stained with two types of fluorescence were stacked five times in alternating layers of 10 layers each using the CAViTs method. The results confirmed that the CAViTs method can be used to construct a 3D cellular tissue structure consisting of multiple cell layers. The average thickness of the tissue was 817 μm, which could be seen with the naked eye (Fig. 1i and j, Fig. S1). Although tissue prepared with heparin alone was thicker, it contained numerous voids and was considered to be immature as tissue (Fig. 1l). In the case of collagen alone, the tissue was thinner than in the case of heparin alone, and no voids were observed in the tissue (Fig. 1m). CAViTs performed using a combination of both heparin and collagen produced the thickest and most void-free tissue (Fig. 1n).

The CAViTs method was also performed using a variety of heparin and collagen combinations, as well as other material combinations, and the results are shown in Table 1. We expected that the combination of cell adhesion ECM and the counterpart biomolecules possessing interaction with the ECM. Thus, common cell adhesive ECMs such as collagen type I, laminin, and fibronectin were selected and then counterpart glycosaminoglycan ECM components such as heparin, chondroitin sulfate A, chondroitin sulfate C, dermatan sulfate and hyaluronic acid were chosen. A polyelectrolyte such as dextran sulfate, polystyrene sulfonic acid and polyacrylic acid were selected as a control polymer of the glycosaminoglycans because of the same negative charges. The thickness of tissue sections and the cell density in the tissues on day 1 of cultures prepared for each combination are shown in Table 1. The solvent of the glycosaminoglycan or polyelectrolyte and extracellular adhesion factor, Tris–HCl buffer exhibited relatively higher tissue thickness (163 μm) and density (69.5 cells/5×10^3 μm^2). Compared with nontreatment (i.e., using Tris–HCl buffer alone), the thickness of the glycosaminoglycan- or polyelectrolyte-only tissue was approximately 1.7-fold greater for heparin, 1.4-fold greater for dermatan sulfate and polyacrylic acid, 1.3-fold greater for chondroitin sulfate C and polystyrene sulfonic acid, and 1.2-fold greater for hyaluronic acid. However, the thickness of tissues observed using dextran sulfate and chondroitin sulfate A were approximately 0.7-fold thinner than that obtained with nontreatment. For all glycosaminoglycans and polyelectrolytes, multiple voids were observed in the tissue (Fig. S2), and cell density decreased by 0.72- to 0.96-fold, indicating a trend toward a decrease in cell density in the tissue (i.e., an increase in tissue thickness).

In contrast, the thickness of tissue prepared with adhesion factor alone was 1.17-fold greater than that prepared with collagen type I alone, and tissue prepared with laminin or fibronectin was almost as thick as nontreatment. In general, tissues prepared with adhesion factor alone had a higher cell density than those prepared with glycosaminoglycan or polyelectrolyte alone, and no voids were generated in the tissues (Fig. S2).

When tissues were prepared using a combination of glycosaminoglycans or polyelectrolytes and adhesion factors, all tissues were thicker when collagen type I was used. Chondroitin sulfate A in combination with collagen type I resulted in a 2.8-fold thickening of tissue compared with nontreatment, and dermatan sulfate resulted in a 2.6-fold tissue thickening. Furthermore, no voids were formed in the tissues prepared with all combinations (Fig. S2). In addition, the combination of heparin and collagen exhibited the best viscous body formation (data not shown).

When cells were stacked in culture medium without treatment with collagen, ECM, or Tris–HCl buffer as a solvent, the thickness was 80 μm (i.e., it was the thinnest), and the cell density was 83.3 cells/5×10^3 μm^2. During the culture medium change, cells did not adhere to each other, resulting in the peeling off of cells; thus, the culture could not be maintained (data not shown).

By a trial-and-error approach, we finally found that combination of heparin and collagen is the suitable for tissue formation.

3.2. Self-assembly of the vascular network in CAViTs

When fibroblasts and vascular endothelial cells were mixed and treated using the CAViTs method as shown in Fig. 2a, HUVECs self-assembled into a capillary morphogenesis network, which devel-

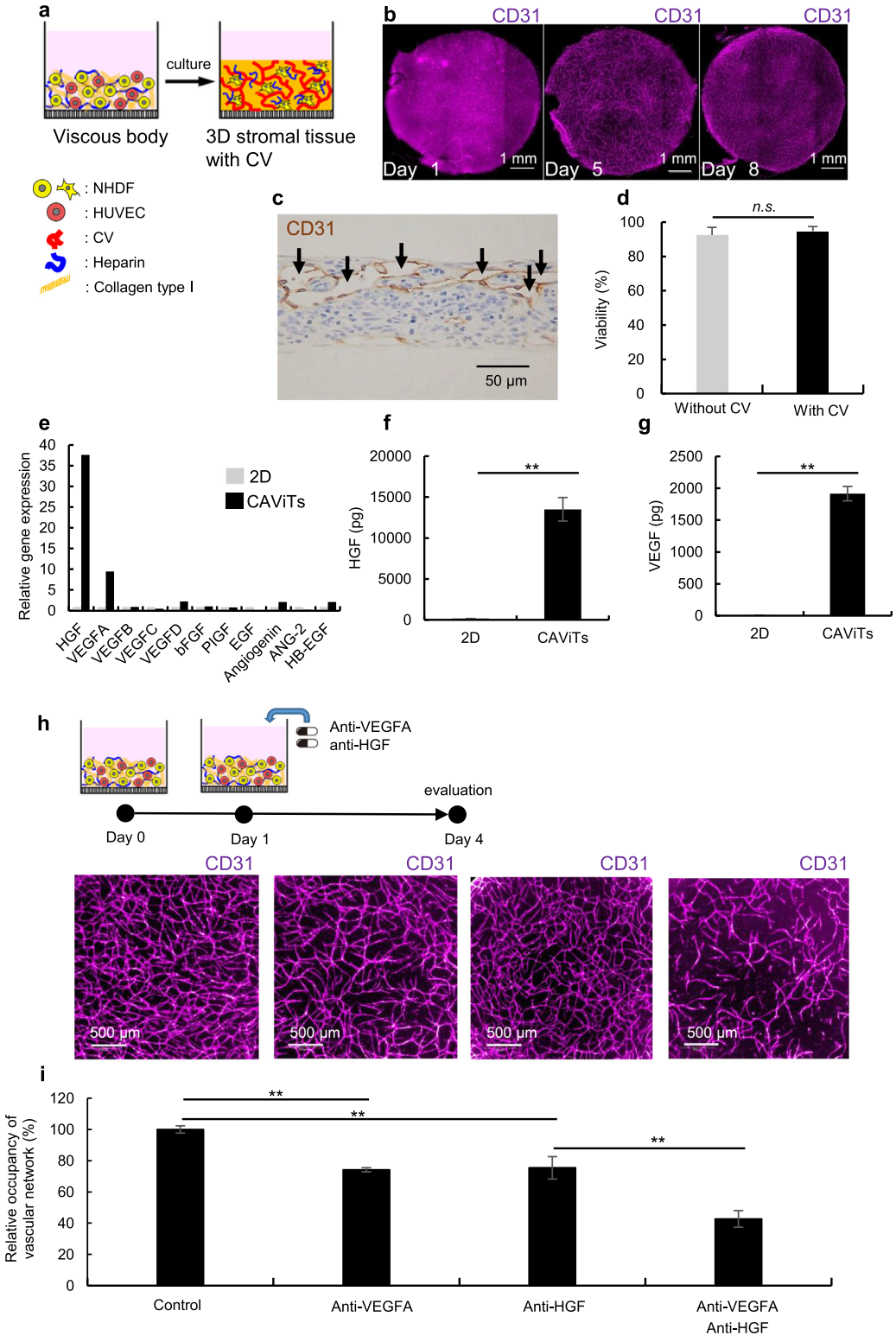

Fig. 2. Self-assembly of vascular network by CAViTs.
Flow diagram of 3D stromal tissue formation with capillary morphogenesis network structure from NHDFs and HUVECs in a mixed viscous body produced using the CAViTs method (a). Immunofluorescence images of changes in the capillary morphogenesis network structure over time (magenta: CD31) on days 1, 5, and 8 of culture (b). IHC image of HUVECs lumen structure on day 8 of culture (brown: CD31, arrows: luminal structures) (c). Overall tissue viability (%) (gray: with capillary morphogenesis vessel [CV], black: without CV) (d). Comparison of angiogenic factor marker expression in 2D versus CAViTs culture methods (CAViTs) determined using microarray gene expression analysis (gray: CAViTs, black: 2D) (e). Comparison of 2D and CAViTs culture methods in terms of HGF (f) and VEGF (g) expression levels by ELISA (gray: 2D, black: CAViTs). Immunofluorescence images of each condition on day4 in the verification of inhibition of vascular network formation using anti-HGF and -VEGF antibodies (magenta: CD31, left: control, left center: anti-VEGFA treated, right center: anti-HGF treated, right: both anti-VEGFA and anti-HGF treated) (h). Relative occupancy of vascular network (%) (measured values for each condition/CD31-derived fluorescence occupancy of control × 100) (i). $^{**}P<0.05$; n.s.: not significant.

oped over time (Fig. 2b). The network was formed when HUVECs were present at >0.25 % relative to NHDFs at day 5 of culture, and the degree of development was HUVEC concentration dependent (Fig. S3). In addition, cross-sectional observation suggested the formation of vessels with open lumens (Fig. 2c). However, as the number of vessels in tumor tissue is reportedly in the range of dozens per field of view, we decided upon a concentration of HUVECs of 1.5 % of total stromal cells in consideration of reproducibility [44].

The overall cell viability was 92.5 % in the tissue composed of only NHDFs and 94.7 % in the tissue composed of self-assembled HUVECs in NHDFs at day 8 of culture, with no significant difference observed depending on the presence or absence of capillary morphogenesis vessels (Fig. 2d). Moreover, the development of the capillary-like structures in stromal tissues exhibited high reproducibility (Fig. S4).

Next, 20 cell layers of stromal tissue composed of NHDFs and HUVECs prepared by the CAViTs method were subjected to DNA microarray analysis to extract a group of genes related to angiogenesis and compared with 2D culture (Fig. 2e). At day 4 of culture and after stromal tissue preparation, expression of the HGF and VEGFA genes was upregulated 37-fold and 9-fold, respectively, compared to 2D cultures. Based on these results, ELISA quantification of HGF and VEGF proteins in stromal tissues prepared by the CAViTs method at day 4 post-culture showed that secretion of HGF and VEGF had increased by 274- and 88-fold, respectively, compared to 2D cultures (Fig. 2f, g).

Next, we evaluated whether formation of the vascular network in the stromal tissue could be inhibited by anti-HGF and anti-VEGF antibodies (Fig. 2h, i). Treatment with either antibody alone inhibited vascular network formation by ~20 %, and the simultaneous addition of both antibodies inhibited the formation of vascular networks by 57.4 % compared with no addition of antibodies. These results showed that vascular networks self-assembled in stromal tissues composed of NHDFs and HUVECs prepared using the CAViTs method, primarily via the HGF and VEGF pathways. In contrast, in tissues prepared using conventional 3D cell culture techniques, the spheroids failed to form a vascular network, and no lumens could be identified (Fig. S5).

3.3. Evaluation of morphology in cancer cell line models generated using CAViTs

Fig. 3 shows a cancer-stromal model with NCI-H1975 lung cancer cells generated using the CAViTs method. The figure shows a model with cancer cells seeded in the upper part of the stroma (Fig. 3a, b) and another model with cancer cells sandwiched between the stromal tissues (Fig. 3c, d). In both cases, the cancer cells were maintained for 7 days with controlled cancer cell positioning. An IHC image of colon cancer HT29 cells seeded on the upper surface of the stromal tissue is shown in Fig. 3e, and NCI-N87 gastric cancer cells sandwiched in the stromal tissue are shown in Fig. 3f. When the gastric cancer cells were sandwiched between the stromal tissues, the glandular duct structure that is typically observed in highly differentiated carcinomas was reconstructed. Some PDCs originating from the colorectal cancer also formed duct structures when they were sandwiched in stromal tissue (Fig. S6). Furthermore, in this model, some colon cancer cells co-localized with the capillary morphogenesis vessels formed in the stromal tissue (Fig. 3g, Fig. S7).

3.4. Evaluation of drug efficacy against cancer cell line models

Fig. 4a shows the anticancer drug evaluation scheme using the cancer-stromal model with cell lines prepared using the CAViTs method. After stromal cells were precipitated in a container using the CAViTs method, cancer cells pre-stained with PKH were seeded on the following day, and the anticancer drug was added on day 5. On day 8, the tissue was digested with trypsin, and the number of residual cancer cells was determined. The percentage of residual HT29 cells in 10 μg/mL and 100 μg/mL of L-OHP alone was 39.4 % and 16.0 % for 2D cultures, 48.2 % and 22.3 % for spheroids, and 62.6 % and 33.8 % for CAViTs, respectively, showing a concentration-dependent trend (Fig. 4b). The effect of L-OHP was the lowest when assayed using the CAViTs method model. Furthermore, when L-OHP was used simultaneously with an angiogenesis inhibitor (anti-VEGF antibody), the combined effect of the anti-VEGF antibody was confirmed at each L-OHP concentration, but only in tissues prepared using the CAViTs method. Note that the anti-VEGF antibody alone had no cytocidal effect in this system (data not shown).

In the cancer-stromal model generated using the CAViTs method with HCT116 cells, a combined effect with angiogenesis inhibitors was observed when HUVECs were present. Compared to the non-vascularized model, the vascularized cancer stromal model was more resistant (by 17.7 %) to 5-FU at 1000 μM. The non-vascularized model did not show any combined effect with the anti-VEGF antibody (Fig. 4c). Furthermore, when the percentage of HUVECs relative to NHDFs was increased in the same system, the combined effect of the anti-VEGF antibody and 5-FU was confirmed with ≥0.5 % HUVECs with good vascular network formation (Fig. 4d).

Next, we examined whether immunostaining could also be used to detect cancer cells co-cultured with stromal tissue. In a preliminary study, a correlation was observed between the areas of detection when PDCs were assessed with the expressed mKate protein and when stained with the cancer cell–specific antibody EpCAM (Fig. S8). We then evaluated the efficacy of four anticancer drugs in the cancer-stromal model by immunostaining and imaging analysis using HT115 colorectal cancer cells in 96-well plates, and compared the efficacy with that in 2D culture (Fig. 5a). The reproducibility of this model obtained from three independent trials was the same as that of 2D cultures (Fig. 5b–e). Co-cultures with stromal tissue were found to be more resistant to all four drugs than was observed in 2D cultures. Specifically, compared to the 2D cultures, the co-cultures were approximately 10-fold more resistant to oxaliplatin, 5-FU, and SN-38, and 1000-fold more resistant to the molecular-targeted drug cetuximab (Fig. 5f, g, Fig. S9).

In addition, three trials of three drugs (afatinib [Afb], osimertinib [OSIM], and cisplatin [CDDP]) were performed against NCI-H1975 lung cancer cells. As with colon cancer cells, the model with NCI-H1975 cells showed high reproducibility, and co-cultures with stromal tissue exhibited greater drug resistance than 2D cultures (Fig. S10).

3.5. PDC-stromal model generated using the CAViTs method and evaluation of anticancer drugs

The results of IHC evaluation of the colon PDC-stromal model prepared using the CAViTs method on day 7 of culture are shown in Fig. 6a. Cancer cells were observed inside the duct structures consisting of HUVECs in multiple sites, suggesting infiltration into vessels (Fig. 6b). In another case of PDCs, on the second day of culture, some of the cancer cells formed glandular duct structures (arrowheads in Fig. 6c). The entire area was raised, and the nuclei of the cancer cells could be clearly seen on the stromal side (dashed circle in Fig. 6d).

Next, drug sensitivity was evaluated using the colon PDC-stromal model. The results shown in Fig. 6e confirmed the combined effect of 5-FU and anti-VEGF antibody against PDCs as well as in the cell line, with a concentration-dependent increase ob-

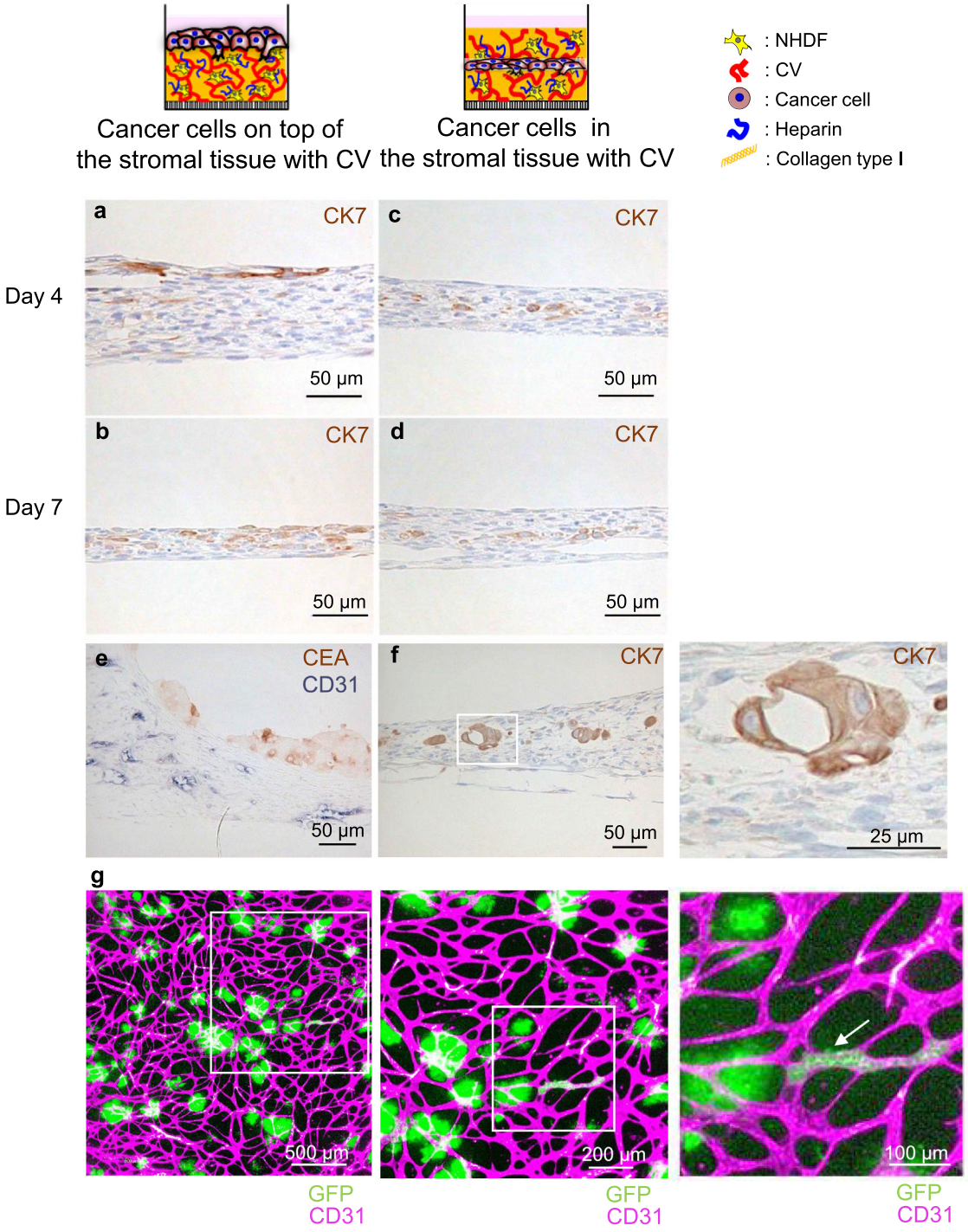

Fig. 3. Morphological evaluation of cancer cell line models generated using CAViTs.
IHC images of NCI-H1975 lung cancer cells on stromal tissue with CV (a: culture day 4, b: culture day 7). IHC images of NCI-H1975 lung cancer cells in the stromal tissue with CV (c: culture day 4, d: culture day 7). IHC image of tissue with HT29 colon cancer cells on top of the stromal tissue after 7 days of culture (brown: CEA, gray: CD31) (e). IHC image of NCI-N87 gastric cancer cells in the stromal tissue after 7days of culture (brown: CK7, white inset: glandular duct structure) and enlarged part of the white inset (f). Observation of cancer cell invasion into CV (green: cancer cells expressing GFP, red: RFP-HUVECs, from left to right, images magnified ×1, ×2.5, ×5, arrow: cancer invasion area) (g).

served in the effect of 5-FU as a single agent. However, the anti-tumor effect of 5-FU was enhanced when combined with the anti-VEGF antibody. We confirmed that the addition of bevacizumab, an angiogenesis inhibitor, resulted in development of a less-sparse vascular network in the stromal tissue compared to no addition of bevacizumab, but a dense vascular network was maintained around the cancer cells (Fig. 6f, g, Fig. S11).

Next, we evaluated drug efficacy in the cancer-stromal co-culture model generated using the CAViTs method with PDCs linked to clinical information. Drug treatment of each PDC line utilized the same combination of drugs used in the patients' original treatment, as described in the experimental section. Table 2 shows the results of comparisons between the efficacy of the evaluated drugs in the CAViTs co-culture model and the predicted ef-

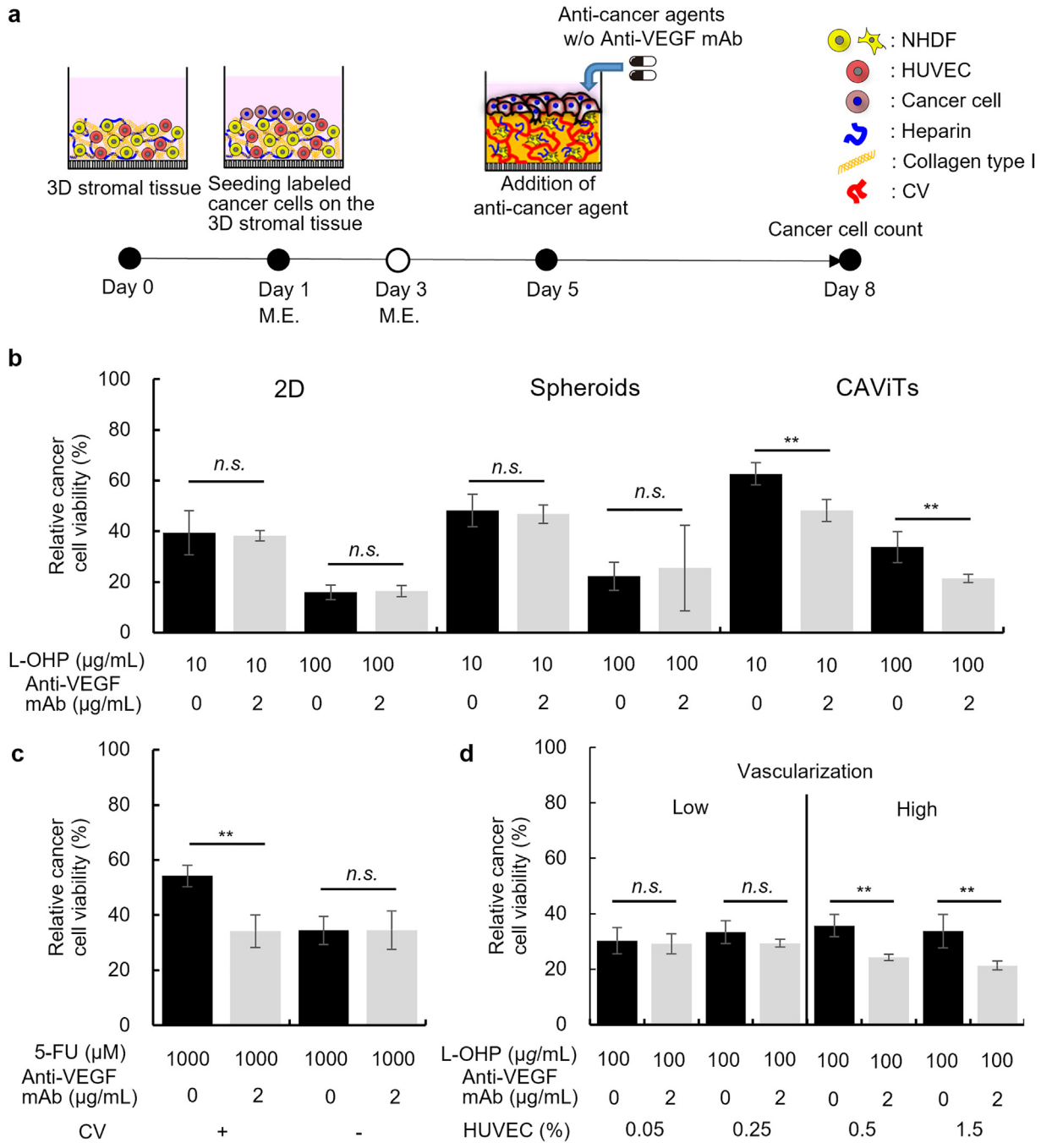

Fig. 4. Evaluation of drug efficacy using cancer cell line models generated by the CAViTs method.
Flow diagram of the procedure of anticancer drug evaluation using the cancer-stromal model (a).Comparison of drug efficacy evaluation results between culture methods (black: L-OHP only, gray: L-OHP+VEGF monoclonal antibody [mAb], HT29) (b). Comparison of drug efficacy evaluation results between with and without CV (black: 5-FU only, gray: 5-FU+VEGF mAb, HCT116) (c). Comparison of efficacy evaluation results for HUVEC content (black: L-OHP only, gray: L-OHP+VEGF mAb, HCT116) (d). $^{**}P<0.05$, n.s.: not significant.

ficacy from clinical outcomes. For the recurrence of liver metastasis (JC-039-2-Liv and JC-054-3-Liv), the PDCs were predicted to be insensitive to the drugs, because they had been established from recurring tumors during treatment. As expected, the drugs were not effective against these PDCs in the model generated using the CAViTs method. Treatment of the metastatic tumor after resection of the primary tumor enabled control of the disease, such that the PDCs established from primary tumors (JC-063-1-TS, JC-075-1-TS, and JC-119-1-TR) were predicted to be sensitive to the drugs. In contrast, the PDCs from the remaining tumors (JC-072-2-Liv, JC-075-2-Liv, and JC-119-2-Liv) were predicted to be insensitive to the drugs because these cell lines originated from tumors that survived treatment and were considered resistant to the drugs. In two of the three PDCs from primary tumors, the drug treatments were effective, as expected from clinical outcomes; however, the result for the other PDC line was not concordant with this expectation. Similarly, as expected, the evaluation showed that the drug treatments were not effective against two of the three PDCs derived from patients in which liver metastasis remained; however, for the other PDC, the result did not match the prediction. The concordance

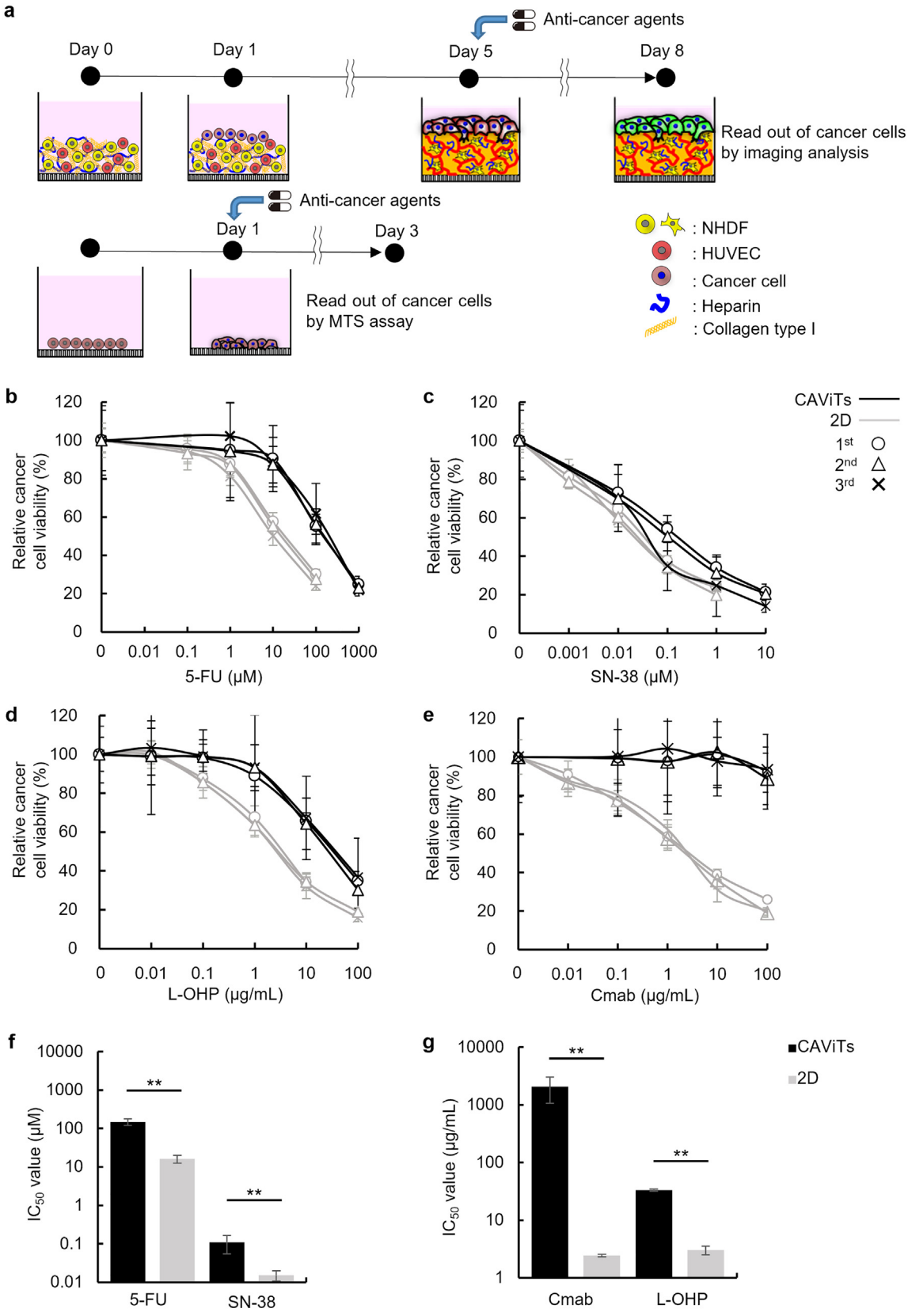

Fig. 5. Reproducibility of drug efficacy evaluations for cancer cell line models generated using the CAViTs method.
Flow diagram of the procedure of anticancer drug evaluation (above: cancer-stromal model, bottom: 2D culture) (a). Comparison of reproducibility of drug efficacy evaluations in three independent trials (1st to 3rd) of the CAViTs method and the 2D culture method (HT115 cells) in 96-well plates(b: 5-FU, c: SN-38, d: L-OHP, e: Cmab , black: CAViTs, gray: 2D). IC_{50} values of 5-FU and SN-38 (f), Cmab and L-OHP (g). $^{**}P < 0.05$.

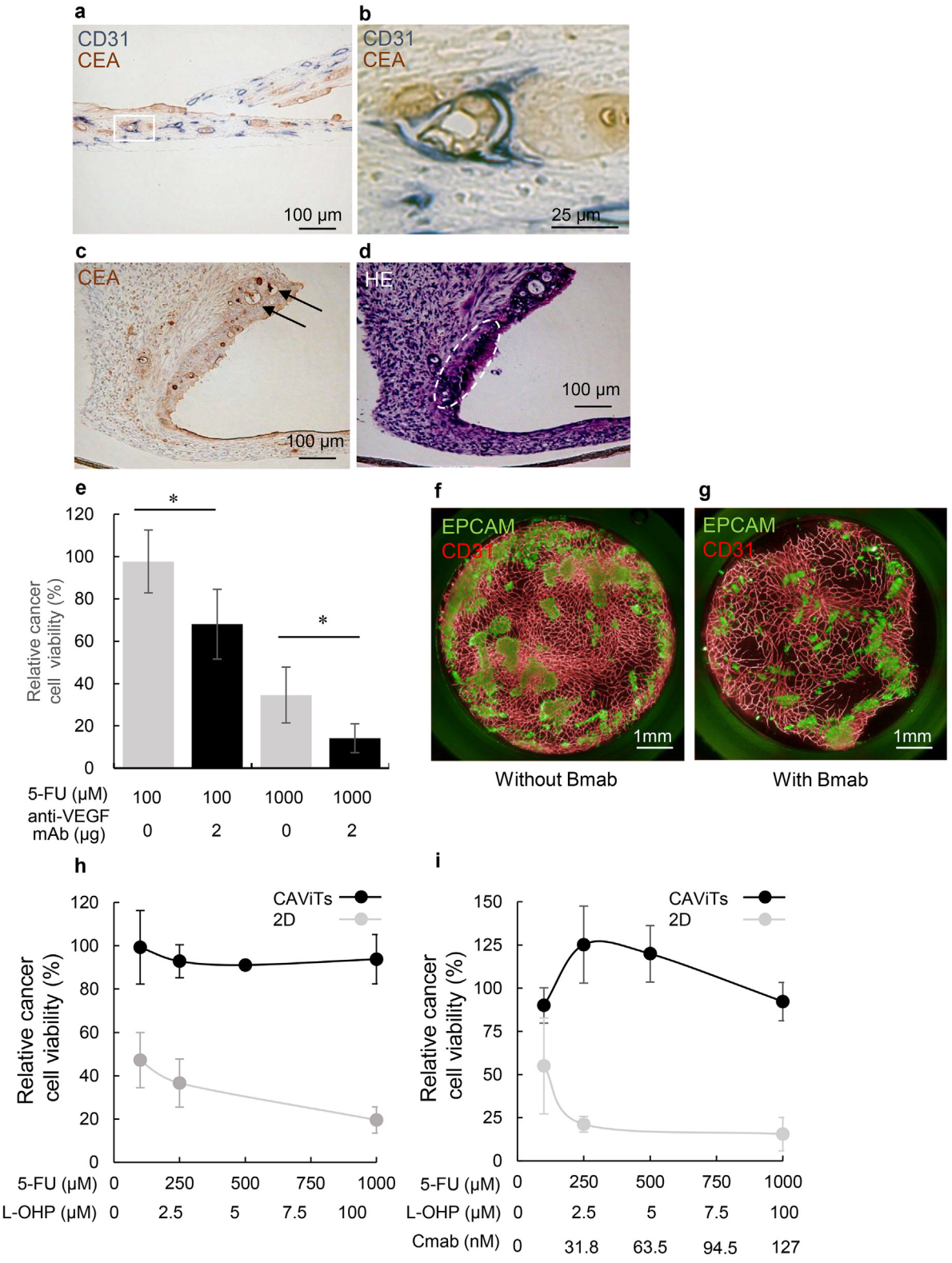

Fig. 6. Construction of PDC-stromal models using the CAViTs method and evaluation of drug efficacy.
IHC images of colorectal JC-143-1-stromal models generated using the CAViTs method (brown: CEA, gray: CD31, white inset: cancer invasion into luminal structure formed with HUVECs) (a) and enlarged image of the cancer invasion area (b). IHC images of colorectal JC-143-1–stromal models (brown: CEA, arrow: glandular duct structure) (c). HE image (dashed white area: nucleus of cancer cells on the stromal side) (d). Results of drug efficacy evaluation using colorectal JC-143-1-stromal models (black: 5-FU only, gray: 5-FU+VEGF antibody) (e). Immunofluorescence images of colorectal JC-143-1–stromal models with and without Bmab (green: EpCAM, red: CD31) (f, g). Comparison of the results of efficacy evaluations of a two-drug combination (5-FU+L-OHP) between the CAViTs method and 2D culture method (black: CAViTs, gray: 2D) (h). Comparison of the results of efficacy evaluation of a three-drug combination (5-FU+L-OHP+Cmab) (black: CAViTs, gray: 2D) (i). *:0.05<P<0.1.

Table 2
Evaluation of drug efficacy in eight PDC cases.

PDCs ID	Clinical information			Predicted efficacy**	Evaluated efficacy (CAViTs)	Concordance
	Organ site	Combination of drugs in chemotherapy	Outcomes*/timing of surgery			
JC-039-2-Liv	Recurrent liver metastasis	mFOLFOX6	PD/post-treatment	Not effective	Not effective	Match
JC-054-3-Liv	Recurrent liver metastasis	mFOLFOX6 + Bmab	PD/post-treatment	Not effective	Not effective	Match
JC-063-1-TS	Sigmoid colon (Primary)	mFOLFOX6 + Cmab	SD/pre-treatment	Effective	Effective	Match
JC-072-2-Liv	Residual liver metastases	mFOLFOX6 + Cmab	PR/post-treatment	Not effective	Not effective	Match
JC-075-1-TS	Sigmoid colon (Primary)	mFOLFOX6 + Cmab	PR/pre-treatment	Effective	Not effective	Mismatch
JC-075-2-Liv	Residual liver metastases	mFOLFOX6 + Cmab	PR/post-treatment	Not effective	Not effective	Match
JC-119-1-TR	Rectum (Primary)	FOLFOXIRI + Bmab	PR/pre-treatment	Effective	Effective	Match
JC-119-2-Liv	Residual liver metastases	FOLFOXIRI + Bmab	PR/post-treatment	Not effective	Effective	Mismatch

Evaluated as mean ± SE of 3 or 4 independent trials. PD: progression of disease, SD: stable disease, PR: partial response. Bmab: bevacizumab, Cmab: cetuximab. In the case of JC-075-1-TS and JC-075-2-Liv, and JC-119-1-TR and JC-119-2-Liv, tumor tissue specimens were obtained from the same patients.

* Clinical outcomes according to RECIST guideline were determined in terms of tumor volume of metastatic lesions.

** Drug treatment of PDCs established from pre-treatment primary tumors was predicted to be effective. For the other PDCs (from post-treatment metastatic tumors), treatment was predicted to be ineffective.

rates in the cases of recurrence during treatment, primary tumor before treatment, and metastatic tumor remaining after treatment were 100 % (2/2), 67 % (2/3), and 67 % (2/3), respectively, with an overall concordance rate of 75 % (6/8). The high concordance rate with clinical outcomes indicates that using the co-culture model generated according to the CAViTs method could be useful for predicting the treatment response of patient tumors.

3.6. Primary cancer cultures of stromal tissues generated using the CAViTs method

This study investigated the feasibility of culturing specimens excised from colorectal cancer patients on 3D stromal tissue in primary culture. Specimens excised from the patient's tumor, fluorescently labeled with PKH before culture, showed increased initial growth on HUVEC feeder conditions without the CAViTs method, indicating the influence of scaffold. However, it showed limited growth over time as well as in both 2D culture. In contrast, cancer cells cultured on 3D stromal tissue demonstrated substantial proliferation. Interestingly, cancer cells displayed increased proliferation in vascularized stromal tissue compared to non-vascularized tissue (Fig. 7a, b). To verify that PKH-labeled cells were indeed cancer cells, specific markers for cancer cells were assessed. Primary cells from JC-278, cultured on 3D stromal tissue, exhibited strong staining for CEA and EpCAM, confirming the presence and proliferation of cancer cells (Fig. 7c). Additionally, we observed that cancer cells from case JC-247 proliferated in a stromal tissue fibroblast layer in a number-dependent manner (Fig. 7d). In the case of JC-406, cancer cells demonstrated more efficient proliferation in an HUVEC-percentage or vascular network-dependent manner (Fig. 7e).

4. Discussion

In this study, we developed the CAViTs method, which is a simpler and more rapid method for producing thicker tissues than the previously reported LbL method [39]. The CAViTs method requires only two centrifugation steps compared to the LbL method, resulting in much less damage to cells and a higher cell yield. We previously reported that heparin added to cells in culture forms a viscous medium in a cationic environment [42], but in this study, we found that the agglutination effect of heparin disappears when the viscous medium is resuspended in normal culture medium. The combination of ECM components such as collagen type I is important for maintaining the agglutination effect, even after resuspension of the viscous material in the culture medium, and we showed a relationship between the agglutination effect and stable production of thick tissues. The selected ECM components such as collagen, fibronectin and laminin have well known cell adhesion properties by the interaction with specific integrins. For example, fibronectin generally has an interaction with $\alpha 5\beta 1$ integrin which typically expresses on mesenchymal cell surfaces, and laminin generally has an interaction with $\alpha 1\beta 1$ integrin which is typically expresses on epithelial and endothelial cell surfaces. Accordingly, depending on the target cells for tissue construction, we can choose favorable ECM components. However, it does not mean a limitation of the CAViTs technology.

Additionally, our stromal model consists of NHDFs and HUVECs because they are accessible and reproducible, and the method has been used in previous studies involving the LbL method [39]. To mimic the complex cancer microenvironment, both NHDFs and cancer-associated fibroblasts (CAFs) should be used. Some reports indicate that CAFs exhibit heterogeneity in many cancer types have led to the definition of numerous CAF subtypes. Further studies are thus needed to accurately mimic the cancer microenvironment, taking into account CAF heterogeneity in each cancer type [45,46].

Similar to the LbL method, stromal tissues generated using the CAViTs method were able to self-assemble a vascular network, and comprehensive gene expression analysis of stromal tissues generated using the CAViTs method showed that MMP1 expression was nine-fold higher when vessels were present than when they were absent, indicating that the stroma was easily digestible (data not shown). The results of this analysis showed that the interstitium is more easily digested. As the migration of stroma and HUVECs has been reported [47], it is thought that the environment in this model is also conducive to the migration of HUVECs.

Capillary morphogenesis vessels play an important role in tumor progression, angiogenesis, and metastasis in the cancer microenvironment [48–53]. In the present study, vascular invasion of cancer cells was observed when cells were cultured in CAViTs-generated tissue, and expression of the TGF-β gene in CAViTs-generated stromal tissue was three- to five-fold higher compared to the absence of stromal tissue. We also identified HGF and VEGF as the primary pathways for angiogenesis in this model; TGF-β and HGF reportedly induce epithelial-mesenchymal transition (EMT) in cancer cells [54,55]. Therefore, in our cancer-stromal model, cancer cells likely migrate and induce vascular and tissue invasion.

Cancer-stromal models generated using the CAViTs method tended to be more resistant to anticancer drugs than 2D cultures. One possible reason for this observation is the HGF-dependent drug resistance of cancer cells. HGF-dependent regulatory mechanisms have been reported in cancers of the lung and other tissues [56,57], and they are considered to functionally mimic those of living organisms. In addition, mouse HGF cannot bind to the hu-

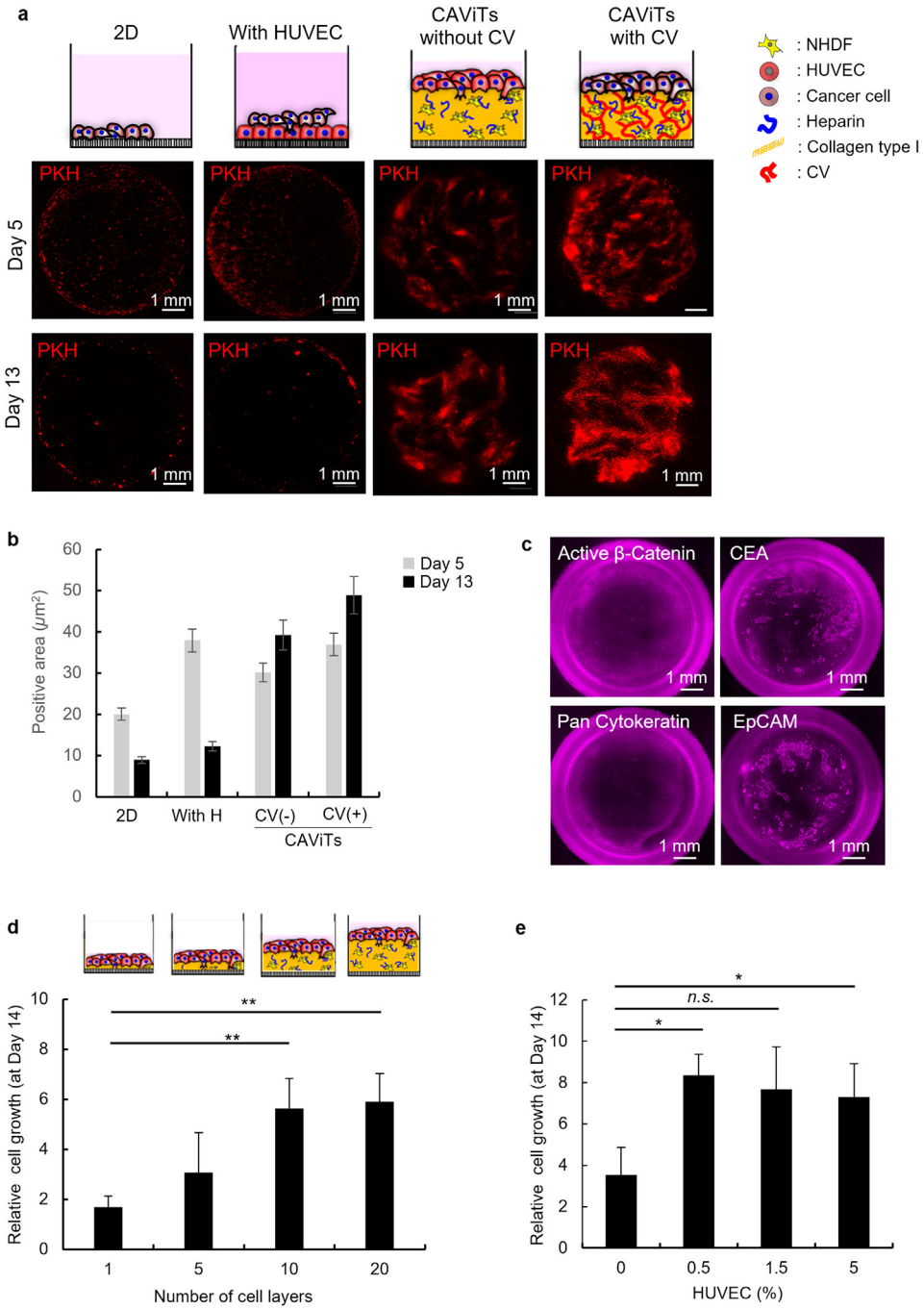

Fig. 7. Primary cancer cell culture of 3D stromal tissue using the CAViTs method.
Fluorescence images of primary cancer cells (JC-115) fluorescently labeled with a PKH26 Red Fluorescent Cell Linker kit with and without CV in 2D culture, in 3D culture using a stromal tissue model generated using the CAViTs method, and cells cultured on a HUVEC feeder and observed over time under each condition (red: PKH) (a). Quantification of PKH-labeled primary cancer cell positive area (gray: Day 5, black: Day 13) (b). Immunofluorescence image of 3D stromal tissue model cultured with JC-278 (magenta: active-β-catenin, CEA, Pan Cytokeratin and EpCAM) (c). Comparison of proliferation rate of JC-247 cells under various numbers of cell layers (1, 5, 10, or 20 layers) (d). Comparison of proliferation rate of JC-406 cells with varying HUVEC content (0, 0.5, 1.5, or 5 %) in the 3D stromal tissue model (e). **:$P<0.05$, *:$0.05<P<0.1$, n.s.: not significant.

man HGF receptor, MET, making the CAViTs method ideal for assessing the critical and precise function of HGF in the cancer microenvironment. Furthermore, it was previously reported that cancer cells undergoing EMT due to TGF-β expression may exhibit reduced proliferation rates and reduced responsiveness to anticancer drugs [58,59].

An important aspect of drug screening is the reproducibility of results. Evaluations of anticancer drug efficacy using the CAViTs system should be considered robust because there were no significant differences among the three trials, as shown in Fig. 5b-e and Supplementary Fig. 10. The lack of standard evaluation methods for co-culture systems, such as ATP and MTS assays, is a major challenge, but this study demonstrated that high content analyses using fluorescent immunostaining can reproducibly evaluate co-culture systems in 96-well plates. This system is therefore considered applicable to high-throughput drug discovery studies. In

the future, automation and adaptation to 384-well plates will enable assays of even greater throughput.

Spheroids also exhibit high morphological reproducibility in terms of control of the diameter of cell clusters, but in the case of co-culture, the positional relationship between cancer cells and stromal tissue is not reproducible due to difficulties in controlling the spatial position of cell clusters, as shown in Supplementary Fig. 5. However, using the CAViTs method, which is a stacking method, cancer cells can be placed in contact with the stromal tissue and maintained in culture for at least 2 weeks. Thus, this method has the potential to generate an orderly *in vivo* microenvironment in which many cells can coexist.

An interesting result of this study was that the cancer stromal model generated using the CAViTs method showed increased efficacy when an angiogenesis inhibitor was combined with cytotoxic agents. One of the reasons for the observed combination effect is that the presence of HUVECs reduces the efficacy of the anticancer drugs. Looking at the phenomenon alone, it appears that as more HUVECs are attacked by the angiogenesis inhibitor, the effectiveness of the anticancer drug increases. Hida *et al.* reported that extracellular vesicles secreted by metastatic tumors induce drug resistance in tumor endothelial cells [60], and it is possible that HUVECs and cancer cells interact in some way. Generally, the combined effect of an angiogenesis inhibitor such as bevacizumab and an anticancer drug is to inhibit angiogenesis and normalize the vascular status of the tumor, which allows the anticancer drug to reach and respond to the tumor. As the capillary morphogenesis vessels near the tumor are rendered abnormal, the pressure in the tumor increases and makes it more difficult for the drug to reach the tumor [61–63]. However, in the cancer stromal model generated using the CAViTs method, functional drugs are delivered via diffusion rather than the vasculature. Therefore, the combination effect observed in this model may be due to a different drug resistance mechanism. If this mechanism can be elucidated, then it may lead to the identification of new molecular targets for angiogenesis inhibitors, which is currently under study.

Stratified medicine, in which two or three drugs are used in combination to treat cancer instead of a single drug, has been proposed as a means of matching the mutational signature of each cancer patient; however, only ~10 % of patients are able to benefit from this approach [64,65]. The reason for this low rate of benefit is that even when active mutations are found, there are often no adaptable molecular-targeted drugs. When considering personalized medicine for such patients, it is useful to construct an *ex vivo* model, or patient avatar, from patient biopsy specimens and evaluate combinations of existing drugs directly on the avatar. In this study, we showed that stromal tissue produced using the CAViTs method can be used for the primary culture of cancer cells from patients with colorectal cancer in normal medium, as shown in Fig. 7. As a high-throughput assay, the CAViTs method model can correctly evaluate anticancer agents in as little as one week, and patient samples can be cultured at low cost with high probability of success without using expensive culture media. On the other hand, the evaluation results of some samples in Table 2 revealed inconsistencies with clinical outcomes. One of the reasons for this discrepancy is the limitation of tissue fabrication via bottom-up approaches, which cannot fully mimic the *in vivo* environment. For instance, the absence of other cells such as immune cells and variations in tissue stiffness may potentially influence drug efficacy [66,67]. Therefore, further research is needed to better mimic the cancer microenvironment in patients and enhance the clinical concordance rate. Regardless, the model generated using this method is also expected to become the ultimate personalized medicine tool in screening for drugs that are effective as single agents or in combination or as a repositioning tool for drug rescue (elucidating new functions) after a failed clinical trial.

5. Conclusion

We constructed a cancer-stromal tissue model in which cancer cells are placed above and inside stromal tissue with vascular network structures derived from vascular endothelial cells in fibroblast tissue using CAViTs, a proprietary tissue engineering technology. Using this method, we were able to reproduce the invasion and metastatic processes of cancer cells observed *in vivo*. Moreover, the addition of 2 μg of Bmab to 100 μM 5-FU in PDCs was found to reduce the survival rate of residual cancer cells by 30 % compared to the single agent, indicating the possibility of evaluating the effect of combination treatment with an angiogenesis inhibitor in tissues with capillary morphogenesis vessels. Importantly, no similar combination effect was observed in 2D cultures or spheroids. In addition, by co-culturing PDCs on stromal tissue, we were able to facilitate the growth of PDCs using normal medium. In eight PDC samples, the effect matched the clinical response to the same drug, and surprisingly, the agreement among the eight samples was 75 %. Furthermore, primary cancer cells also grew on the stromal tissues with the normal medium. These data suggest that the model may be useful for *in vitro* new drug screening and personalized cancer medicine.

Data availability

The data that support the findings of this study are available from the corresponding author, Michiya Matsusaki.

Declaration of competing interest

The authors declare the following financial interests/personal relationships which may be considered as potential competing interests: Michiya Matsusaki, Ryohei Katayama and Eiji Shinozaki report that financial support was provided by TOPPAN Holdings Inc.

Michiya Matsusaki, Ryohei Katayama, Shinji Irie, Satoshi Nagayama and TOPPAN Holdings Inc are inventors of several patents related to the CAViTs method.

Yuki Takahashi, Rii Morimura, Kei Tsukamoto, Sayaka Gomi, Asuka Yamada, Miki Mizukami, Yasuyuki Naito and Shiro Kitano are employees of TOPPAN Holdings Inc.

CRediT authorship contribution statement

Yuki Takahashi: Conceptualization, Data curation, Formal analysis, Investigation, Methodology, Validation, Visualization, Writing – original draft, Writing – review & editing. **Rii Morimura:** Conceptualization, Data curation, Formal analysis, Investigation, Methodology, Validation, Visualization, Writing – original draft, Writing – review & editing. **Kei Tsukamoto:** Conceptualization, Data curation, Formal analysis, Investigation, Methodology, Validation, Visualization, Writing – review & editing. **Sayaka Gomi:** Data curation, Investigation, Methodology, Validation. **Asuka Yamada:** Data curation, Investigation. **Miki Mizukami:** Data curation, Investigation. **Yasuyuki Naito:** Data curation, Investigation. **Shinji Irie:** Data curation, Investigation, Methodology, Validation. **Satoshi Nagayama:** Resources, Writing – review & editing. **Eiji Shinozaki:** Conceptualization, Project administration, Resources, Supervision, Writing – review & editing. **Kensei Yamaguchi:** Resources, Supervision, Writing – review & editing. **Naoya Fujita:** Project administration, Resources, Supervision. **Shiro Kitano:** Conceptualization, Funding acquisition, Methodology, Project administration, Supervision, Writing – review & editing. **Ryohei Katayama:** Conceptualization, Funding acquisition, Project administration, Resources, Supervision, Writing – review & editing. **Michiya Matsusaki:** Conceptualization, Funding acquisition, Methodology, Project administration, Supervision, Writing – review & editing.

Acknowledgments

The authors thank TOPPAN Holdings Inc., to which the authors are affiliated, the Osaka University Joint Research Chair, and the co-authors at Osaka University for their involvement in the experimental design, conducting the experiments, and analyzing the data.

The authors also thank Tomoko Oh-hara of the Cancer Chemotherapy Center, Japanese Foundation for Cancer Research (JFCR), the staff of the Department of Gastrointestinal Surgery, the Cancer Institute Hospital, JFCR, who performed the specimen collection, and the patients who donated surgically resected tumor specimens. The authors acknowledge financial support by a Grant-in-Aid for Scientific Research (A) (20H00665) and a Grant-in-Aid for Challenging Exploratory Research (22K19918) from the JSPS.

Supplementary materials

Supplementary material associated with this article can be found, in the online version, at doi:10.1016/j.actbio.2024.05.037.

References

[1] JPMA DATABOOK 2020_English, 2020, p. 65 http://www.jpma.or.jp/about/issue/gratis/databook/.
[2] C.H. Wong, K.W. Siah, A.W. Lo, Estimation of clinical trial success rates and related parameters, Biostatistics 20 (2019) 273–286, doi:10.1093/biostatistics/kxx069.
[3] J.I. Johnson, S. Decker, D. Zaharevitz, L.V. Rubinstein, J.M. Venditti, S. Schepartz, S. Kalyandrug, M. Christian, S. Arbuck, M. Hollingshead, E.A. Sausville, Relationships between drug activity in NCI preclinical in vitro and in vivo models and early clinical trials, Br. J. Cancer. 84 (2001) 1424–1431, doi:10.1054/bjoc.2001.1796.
[4] T. Voskoglou-Nomikos, J.L. Pater, L. Seymour, Clinical predictive value of the in vitro cell line, human xenograft, and mouse allograft preclinical cancer models, Clin. Cancer Res. (2003) 4227–4239.
[5] E. Izumchenko, K. Paz, D. Ciznadija, I. Sloma, A. Katz, D. Vasquez-Dunddel, I. Ben-Zvi, J. Stebbing, W. McGuire, W. Harris, R. Maki, A. Gaya, A. Bedi, S. Zacharoulis, R. Ravi, L.H. Wexler, M.O. Hoque, C. Rodriguez-Galindo, H. Pass, N. Peled, A. Davies, R. Morris, M. Hidalgo, D. Sidransky, Patient-derived xenografts effectively capture responses to oncology therapy in a heterogeneous cohort of patients with solid tumors, Ann. Oncol. 28 (2017) 2595–2605, doi:10.1093/annonc/mdx416.
[6] K. Sunami, H. Ichikawa, T. Kubo, M. Kato, Y. Fujiwara, A. Shimomura, T. Koyama, H. Kakishima, M. Kitami, H. Matsushita, E. Furukawa, D. Narushima, M. Nagai, H. Taniguchi, N. Motoi, S. Sekine, A. Maeshima, T. Mori, R. Watanabe, M. Yoshida, A. Yoshida, H. Yoshida, K. Satomi, A. Sukeda, T. Hashimoto, T. Shimizu, S. Iwasa, K. Yonemori, K. Kato, C. Morizane, C. Ogawa, N. Tanabe, K. Sugano, N. Hiraoka, K. Tamura, T. Yoshida, Y. Fujiwara, A. Ochiai, N. Yamamoto, T. Kohno, Feasibility and utility of a panel testing for 114 cancer-associated genes in a clinical setting: a hospital-based study, Cancer Sci. 110 (2019) 1480–1490, doi:10.1111/cas.13969.
[7] J.K. Sicklick, S. Kato, R. Okamura, M. Schwaederle, M.E. Hahn, C.B. Williams, P. De, A. Krie, D.E. Piccioni, V.A. Miller, J.S. Ross, A. Benson, J. Webster, P.J. Stephens, J.J. Lee, P.T. Fanta, S.M. Lippman, B. Leyland-Jones, R. Kurzrock, Molecular profiling of cancer patients enables personalized combination therapy: the I-PREDICT study, Nat. Med. 25 (2019) 744–750, doi:10.1038/s41591-019-0407-5.
[8] P. Baluk, J. Fuxe, H. Hashizume, T. Romano, E. Lashnits, S. Butz, D. Vestweber, M. Corada, C. Molendini, E. Dejana, D.M. McDonald, Functionally specialized junctions between endothelial cells of lymphatic vessels, J. Exp. Med. 204 (2007) 2349–2362, doi:10.1084/jem.20062596.
[9] C. Feig, J.O. Jones, M. Kraman, R.J.B. Wells, A. Deonarine, D.S. Chan, C.M. Connell, E.W. Roberts, Q. Zhao, O.L. Caballero, S.A. Teichmann, T. Janowitz, D.I. Jodrell, D.A. Tuveson, D.T. Fearon, Targeting CXCL12 from FAP-expressing carcinoma-associated fibroblasts synergizes with anti-PD-L1 immunotherapy in pancreatic cancer, Proc. Natl. Acad. Sci. U. S. A. 110 (2013) 20212–20217, doi:10.1073/pnas.1320318110.
[10] D. Hanahan, L.M. Coussens, Accessories to the crime: functions of cells recruited to the tumor microenvironment, Cancer Cell 21 (2012) 309–322, doi:10.1016/j.ccr.2012.02.022.
[11] M.R. Junttila, F.J. De Sauvage, Influence of tumour micro-environment heterogeneity on therapeutic response, Nature 501 (2013) 346–354, doi:10.1038/nature12626.
[12] F. Spill, D.S. Reynolds, R.D. Kamm, M.H. Zaman, Impact of the physical microenvironment on tumor progression and metastasis, Curr. Opin. Biotechnol. (2016), doi:10.1016/j.copbio.2016.02.007.
[13] V. Delprat, C. Huart, O. Feron, F. Soncin, C. Michiels, The impact of macrophages on endothelial cells is potentiated by cycling hypoxia: Enhanced tumor inflammation and metastasis, Front. Oncol. (2022) 12, doi:10.3389/fonc.2022.961753.
[14] C. Fotsitzoudis, A. Koulouridi, I. Messaritakis, T. Konstantinidis, N. Gouvas, J. Tsiaoussis, J. Souglakos, Cancer-associated fibroblasts: the origin, biological characteristics and role in cancer—a glance on colorectal cancer, Cancers 14 (2022) 4394, doi:10.3390/cancers14184394.
[15] J. Paulsson, P. Micke, Prognostic relevance of cancer-associated fibroblasts in human cancer, Semin. Cancer Biol. 25 (2014) 61–68, doi:10.1016/j.semcancer.2014.02.006.
[16] L.R. Sanchez, L. Borriello, D. Entenberg, J.S. Condeelis, M.H. Oktay, G.S. Karagiannis, The emerging roles of macrophages in cancer metastasis and response to chemotherapy, J. Leukoc. Biol. 106 (2019) 259–274, doi:10.1002/JLB.MR0218-056RR.
[17] M. Mazzone, G. Bergers, Regulation of blood and lymphatic vessels by immune cells in tumors and metastasis, Annu. Rev. Physiol. 81 (2019) 535–560, doi:10.1146/annurev-physiol-020518-114721.
[18] S. Goel, D.G. Duda, L. Xu, L.L. Munn, Y. Boucher, D. Fukumura, R.K. Jain, Normalization of the vasculature for treatment of cancer and other diseases, Physiol. Rev. 91 (2011) 1071–1121, doi:10.1152/physrev.00038.2010.
[19] V. Brancato, J.M. Oliveira, V.M. Correlo, R.L. Reis, S.C. Kundu, Could 3D models of cancer enhance drug screening? Biomaterials 232 (2020) 119744, doi:10.1016/j.biomaterials.2019.119744.
[20] M. Matsusaki, C.P. Case, M. Akashi, Three-dimensional cell culture technique and pathophysiology, Adv. Drug Deliv. Rev. 74 (2014) 95–103, doi:10.1016/j.addr.2014.01.003.
[21] H. Koike, K. Iwasawa, R. Ouchi, M. Maezawa, K. Giesbrecht, N. Saiki, A. Ferguson, M. Kimura, W.L. Thompson, J.M. Wells, A.M. Zorn, T. Takebe, Modelling human hepato-biliary-pancreatic organogenesis from the foregut–midgut boundary, Nature 574 (2019) 112–116, doi:10.1038/s41586-019-1598-0.
[22] H. Koike, K. Iwasawa, R. Ouchi, M. Maezawa, M. Kimura, A. Kodaka, S. Nishii, W.L. Thompson, T. Takebe, Engineering human hepato-biliary-pancreatic organoids from pluripotent stem cells, Nat. Protoc. 16 (2021) 919–936, doi:10.1038/s41596-020-00441-w.
[23] T. Takebe, J.M. Wells, Organoids by design, Science 364 (2019) 956–959, doi:10.1126/science.aaw7567.
[24] T. Sato, R.G. Vries, H.J. Snippert, M. Van De Wetering, N. Barker, D.E. Stange, J.H. Van Es, A. Abo, P. Kujala, P.J. Peters, H. Clevers, Single Lgr5 stem cells build crypt-villus structures in vitro without a mesenchymal niche, Nature 459 (2009) 262–265, doi:10.1038/nature07935.
[25] S. Ding, C. Hsu, Z. Wang, N.R. Natesh, R. Millen, M. Negrete, N. Giroux, G.O. Rivera, A. Dohlman, S. Bose, T. Rotstein, K. Spiller, A. Yeung, Z. Sun, C. Jiang, R. Xi, B. Wilkin, P.M. Randon, I. Williamson, D.A. Nelson, D. Delubac, S. Oh, G. Rupprecht, J. Isaacs, J. Jia, C. Chen, J.P. Shen, S. Kopetz, S. McCall, A. Smith, N. Gjorevski, A.C. Walz, S. Antonia, E. Marrer-Berger, H. Clevers, D. Hsu, X. Shen, Patient-derived micro-organospheres enable clinical precision oncology, Cell Stem Cell 29 (2022) 905–917.e6, doi:10.1016/j.stem.2022.04.006.
[26] G.E. Wensink, S.G. Elias, J. Mullenders, M. Koopman, S.F. Boj, O.W. Kranenburg, J.M.L. Roodhart, Patient-derived organoids as a predictive biomarker for treatment response in cancer patients, Npj Precis. Oncol. 5 (2021) 30, doi:10.1038/s41698-021-00168-1.
[27] S.F. Roerink, N. Sasaki, H. Lee-Six, M.D. Young, L.B. Alexandrov, S. Behjati, T.J. Mitchell, S. Grossmann, H. Lightfoot, D.A. Egan, A. Pronk, N. Smakman, J. Van Gorp, E. Anderson, S.J. Gamble, C. Alder, M. Van De Wetering, P.J. Campbell, M.R. Stratton, H. Clevers, Intra-tumour diversification in colorectal cancer at the single-cell level, Nature 556 (2018) 437–462, doi:10.1038/s41586-018-0024-3.
[28] S.N. Ooft, F. Weeber, L. Schipper, K.K. Dijkstra, C.M. McLean, S. Kaing, J. van de Haar, W. Prevoo, E. van Werkhoven, P. Snaebjornsson, L.R. Hoes, M. Chalabi, D. van der Velden, M. van Leerdam, H. Boot, C. Grootscholten, A.D.R. Huitema, H.J. Bloemendal, E. Cuppen, E.E. Voest, Prospective experimental treatment of colorectal cancer patients based on organoid drug responses, ESMO Open 6 (2021), doi:10.1016/j.esmoop.2021.100103.
[29] P. Thummarati, W. Laiwattanapaisal, R. Nitta, M. Fukuda, A. Hassametto, M. Kino-oka, Recent advances in cell sheet engineering: from fabrication to clinical translation, Bioengineering 10 (2023) 211, doi:10.3390/bioengineering10020211.
[30] G. Wishart, P. Gupta, G. Schettino, A. Nisbet, E. Velliou, 3D tissue models as tools for radiotherapy screening for pancreatic cancer, Br. J. Radiol. (2021) 94, doi:10.1259/bjr.20201397.
[31] S. Iwai, S. Kishimoto, Y. Amano, A. Nishiguchi, M. Matsusaki, A. Takeshita, M. Akashi, Three-dimensional cultured tissue constructs that imitate human living tissue organization for analysis of tumor cell invasion, J. Biomed. Mater. Res. Part A. 107 (2019) 292–300, doi:10.1002/jbm.a.36319.
[32] H. Oikiri, Y. Asano, M. Matsusaki, M. Akashi, H. Shimoda, Y. Yokoyama, Inhibitory effect of carbonyl reductase 1 against peritoneal progression of ovarian cancer: evaluation by ex vivo 3D-human peritoneal model, Mol. Biol. Rep. 46 (2019) 4685–4697, doi:10.1007/s11033-019-04788-6.
[33] A. Nishiguchi, M. Matsusaki, M.R. Kano, H. Nishihara, D. Okano, Y. Asano, H. Shimoda, S. Kishimoto, S. Iwai, M. Akashi, In vitro 3D blood/lymph-vascularized human stromal tissues for preclinical assays of cancer metastasis, Biomaterials 179 (2018) 144–155, doi:10.1016/j.biomaterials.2018.06.019.
[34] K. Yanagisawa, M. Konno, H. Liu, S. Irie, T. Mizushima, M. Mori, Y. Doki, H. Eguchi, M. Matsusaki, H. Ishii, A four-dimensional organoid system to visualize cancer cell vascular invasion, Biology 9 (2020) 1–14, doi:10.3390/biology9110361.

[35] A. Nishiguchi, H. Yoshida, M. Matsusaki, M. Akashi, Rapid construction of three-dimensional multilayered tissues with endothelial tube networks by the cell-accumulation technique, Adv. Mater. 23 (2011) 3506–3510, doi:10.1002/adma.201101787.
[36] K. Baghy, P. Tátrai, E. Regös, I. Kovalszky, Proteoglycans in liver cancer, World J. Gastroenterol. 22 (2016) 379–393, doi:10.3748/wjg.v22.i1.379.
[37] Y.H. Chen, Y. Narimatsu, T.M. Clausen, C. Gomes, R. Karlsson, C. Steentoft, C.B. Spliid, T. Gustavsson, A. Salanti, A. Persson, A. Malmström, D. Willén, U. Ellervik, E.P. Bennett, Y. Mao, H. Clausen, Z. Yang, The GAGOme: a cell-based library of displayed glycosaminoglycans, Nat. Methods. 15 (2018) 881–888, doi:10.1038/s41592-018-0086-z.
[38] J.T. Gallagher, M. Lyon, W.P. Steward, Structure and function of heparin sulphate proteoglycans, Biochem. J. 236 (1986) 313–325, doi:10.1042/bj2360313.
[39] U. Lindahl, M. Höök, Glycosaminoglycans and their binding to biological macromolecules, Annu. Rev. Biochem. 47 (1978) 385–417, doi:10.1146/annurev.bi.47.070178.002125.
[40] A. Orlidge, P.A. D'Amore, Cell specific effects of glycosaminoglycans on the attachment and proliferation of vascular wall components, Microvasc. Res. 31 (1986) 41–53, doi:10.1016/0026-2862(86)90005-1.
[41] Y. Amano, A. Nishiguchi, M. Matsusaki, H. Iseoka, S. Miyagawa, Y. Sawa, M. Seo, T. Yamaguchi, M. Akashi, Development of vascularized iPSC derived 3D-cardiomyocyte tissues by filtration Layer-by-Layer technique and their application for pharmaceutical assays, Acta Biomater. 33 (2016) 110–121, doi:10.1016/j.actbio.2016.01.033.
[42] Y. Naito, Y. Yoshinouchi, Y. Sorayama, H. Kohara, S. Kitano, S. Irie, M. Matsusaki, Constructing vascularized hepatic tissue by cell-assembled viscous tissue sedimentation method and its application for vascular toxicity assessment, Acta Biomater (2022), doi:10.1016/j.actbio.2021.11.027.
[43] N. Tanaka, T. Mashima, A. Mizutani, A. Sato, A. Aoyama, B. Gong, H. Yoshida, Y. Muramatsu, K. Nakata, M. Matsuura, R. Katayama, S. Nagayama, N. Fujita, Y. Sugimoto, H. Seimiya, APC mutations as a potential biomarker for sensitivity to tankyrase inhibitors in colorectal cancer, Mol. Cancer Ther. (2017), doi:10.1158/1535-7163.MCT-16-0578.
[44] Y. Takahashi, Y. Kitadai, C.D. Bucana, L.M. Ellis, Y. Takahashi, K.R. Cleary, Expression of vascular endothelial growth factor and its receptor, KDR, correlates with vascularity, metastasis, and proliferation of human colon cancer, Cancer Res. 55 (1995) 3969–3972 http://www.ncbi.nlm.nih.gov/pubmed/7664263.
[45] G. Friedman, O. Levi-Galibov, E. David, C. Bornstein, A. Giladi, M. Dadiani, A. Mayo, C. Halperin, M. Pevsner-Fischer, H. Lavon, S. Mayer, R. Nevo, Y. Stein, N. Balint-Lahat, I. Barshack, H.R. Ali, C. Caldas, E. Nili-Gal-Yam, U. Alon, I. Amit, R. Scherz-Shouval, Cancer-associated fibroblast compositions change with breast cancer progression linking the ratio of S100A4+ and PDPN+ CAFs to clinical outcome, Nat. Cancer 1 (2020) 692–708, doi:10.1038/s43018-020-0082-y.
[46] S.Z. Wu, D.L. Roden, C. Wang, H. Holliday, K. Harvey, A.S. Cazet, K.J. Murphy, B. Pereira, G. Al-Eryani, N. Bartonicek, R. Hou, J.R. Torpy, S. Junankar, C. Chan, C.E. Lam, M.N. Hui, L. Gluch, J. Beith, A. Parker, E. Robbins, D. Segara, C. Mak, C. Cooper, S. Warrier, A. Forrest, J. Powell, S. O'Toole, T.R. Cox, P. Timpson, E. Lim, X.S. Liu, A. Swarbrick, Stromal cell diversity associated with immune evasion in human triple-negative breast cancer, EMBO J. 39 (2020), doi:10.15252/embj.2019104063.
[47] K. Sobierajska, W.M. Ciszewski, I. Sacewicz-Hofman, J. Niewiarowska, Endothelial cells in the tumor microenvironment, Adv. Exp. Med. Biol. (2020) 71–86, doi:10.1007/978-3-030-37184-5_6.
[48] K. Hida, N. Maishi, D.A. Annan, Y. Hida, Contribution of tumor endothelial cells in cancer progression, Int. J. Mol. Sci. 19 (2018) 1272, doi:10.3390/ijms19051272.
[49] N. Maishi, D.A. Annan, H. Kikuchi, Y. Hida, K. Hida, Tumor endothelial heterogeneity in cancer progression, Cancers 11 (2019) 1511, doi:10.3390/cancers11101511.
[50] N. Maishi, K. Hida, Tumor endothelial cells accelerate tumor metastasis, Cancer Sci. 108 (2017) 1921–1926, doi:10.1111/cas.13336.
[51] K. Hida, Y. Hida, M. Shindoh, Understanding tumor endothelial cell abnormalities to develop ideal anti-angiogenic therapies, Cancer Sci. 99 (2008) 459–466, doi:10.1111/j.1349-7006.2007.00704.x.
[52] J. Folkman, Role of angiogenesis in tumor growth and metastasis, Semin. Oncol. 29 (2002) 15–18, doi:10.1053/sonc.2002.37263.
[53] L.M. Sherwood, E.E. Parris, J. Folkman, Tumor angiogenesis: therapeutic implications, N. Engl. J. Med. 285 (1971) 1182–1186, doi:10.1056/nejm197111182852108.
[54] D. Jiao, J. Wang, W. Lu, X. Tang, J. Chen, H. Mou, Q.Y. Chen, Curcumin inhibited HGF-induced EMT and angiogenesis through regulating c-Met dependent PI3K/Akt/mTOR signaling pathways in lung cancer, Mol. Ther. Oncol. 3 (2016) 16018, doi:10.1038/mto.2016.18.
[55] K. Matsumoto, T. Nakamura, Hepatocyte growth factor and the Met system as a mediator of tumor-stromal interactions, Int. J. Cancer 119 (2006) 477–483, doi:10.1002/ijc.21808.
[56] M. Razzak, Hepatocyte growth factor—a culprit of drug resistance, Nat. Rev. Clin. Oncol. 9 (2012) 429, doi:10.1038/nrclinonc.2012.124.
[57] S. Yano, W. Wang, Q. Li, K. Matsumoto, H. Sakurama, T. Nakamura, H. Ogino, S. Kakiuchi, M. Hanibuchi, Y. Nishioka, H. Uehara, T. Mitsudomi, Y. Yatabe, T. Nakamura, S. Sone, Hepatocyte growth factor induces gefitinib resistance of lung adenocarcinoma with epidermal growth factor receptor-activating mutations, Cancer Res. (2008), doi:10.1158/0008-5472.CAN-08-1643.I.
[58] I. Fabregat, A. Malfettone, J. Soukupova, New insights into the crossroads between EMT and stemness in the context of cancer, J. Clin. Med. (2016), doi:10.3390/jcm5030037.
[59] B.N. Kim, D.H. Ahn, N. Kang, C.D. Yeo, Y.K. Kim, K.Y. Lee, T.J. Kim, S.H. Lee, M.S. Park, H.W. Yim, J.Y. Park, C.K. Park, S.J. Kim, TGF-β induced EMT and stemness characteristics are associated with epigenetic regulation in lung cancer, Sci. Rep. (2020), doi:10.1038/s41598-020-67325-7.
[60] C. Torii, N. Maishi, T. Kawamoto, M. Morimoto, K. Akiyama, Y. Yoshioka, T. Minami, T. Tsumita, M.T. Alam, T. Ochiya, Y. Hida, K. Hida, miRNA-1246 in extracellular vesicles secreted from metastatic tumor induces drug resistance in tumor endothelial cells, Sci. Rep. (2021), doi:10.1038/s41598-021-92879-5.
[61] B.P. Eliceiri, R. Paul, P.L. Schwartzberg, J.D. Hood, J. Leng, D.A. Cheresh, Selective requirement for Src kinases during VEGF-induced angiogenesis and vascular permeability, Mol. Cell. (1999), doi:10.1016/S1097-2765(00)80221-X.
[62] R.K. Jain, R.T. Tong, L.L. Munn, Effect of vascular normalization by antiangiogenic therapy on interstitial hypertension, peritumor edema, and lymphatic metastasis: Insights from a mathematical model, Cancer Res. (2007), doi:10.1158/0008-5472.CAN-06-4102.
[63] S.M. Weis, D.A. Cheresh, Pathophysiological consequences of VEGF-induced vascular permeability, Nature (2005), doi:10.1038/nature03987.
[64] T. Kou, M. Kanai, Y. Yamamoto, M. Kamada, M. Nakatsui, T. Sakuma, H. Mochizuki, A. Hiroshima, A. Sugiyama, E. Nakamura, H. Miyake, S. Minamiguchi, K. Takaori, S. Matsumoto, H. Haga, H. Seno, S. Kosugi, Y. Okuno, M. Muto, Clinical sequencing using a next-generation sequencing-based multiplex gene assay in patients with advanced solid tumors, Cancer Sci. (2017), doi:10.1111/cas.13265.
[65] H. Hayashi, S. Tanishima, K. Fujii, R. Mori, C. Okada, E. Yanagita, Y. Shibata, R. Matsuoka, T. Amano, T. Yamada, I. Yabe, I. Kinoshita, Y. Komatsu, H. Dosaka-Akita, H. Nishihara, Clinical impact of a cancer genomic profiling test using an in-house comprehensive targeted sequencing system, Cancer Sci. (2020), doi:10.1111/cas.14608.
[66] M. Kalli, M.D. Poskus, T. Stylianopoulos, I.K. Zervantonakis, Beyond matrix stiffness: targeting force-induced cancer drug resistance, Trends in Cancer 9 (2023) 937–954, doi:10.1016/j.trecan.2023.07.006.
[67] Y. Meng, H. Wang, X. Li, X. Wu, H. Sun, Editorial: Immunity in the development of anti-cancer drug resistance, Front. Pharmacol. 13 (2022). doi:10.3389/fphar.2022.1120037.